NASA Technical Memorandum 104587

Normal Modes of the World's Oceans
A Numerical Investigation Using Proudman Functions

Braulio V. Sanchez
NASA Goddard Space Flight Center
Greenbelt, Maryland

Dennis Morrow
Cray Research, Inc.
Beltsville, Maryland

National Aeronautics and
Space Administration

Goddard Space Flight Center
Greenbelt, Maryland 20771

1993

PREFACE

This work deals with the numerical modeling of the normal modes of the global oceans. The results of such modeling could be expected to serve as a guide in the analysis of observations and measurements intended to detect these modes. The numerical computation of normal modes of the global oceans is a field in which several investigations have obtained results during the past 15 years. The results seem to be model-dependent to an unsatisfactory extent. This work addresses some modeling areas, such as higher resolution of the bathymetry, inclusion of self-attraction and loading, the role of the Arctic Ocean, and systematic testing by means of diagnostic models. The results show that the present state of the art is such that a final solution to the normal mode problem still lies in the future. The numerical experiments show where some of the difficulties are and give some insight as to how to proceed in the future.

INTRODUCTION

This paper deals with the numerical modeling of the normal modes of the global oceans. In addition to its intrinsic interest as a problem in applied mathematical physics, the results of such modeling could be expected to serve as a guide in the analysis of observations and measurements intended to detect these modes. The observation of the modes is important for a number of reasons, such as the understanding of the oceans's response to forcing by gravitational forces (tides), wind stresses (circulation), and perhaps even to changes in the rotational potential of the Earth (pole tide). The numerical computation of normal modes of the global oceans is a field in which several investigations have obtained results during the past 15 years. These will be cited in the text below. As indicated by Platzman (1991), the results seem to be model-dependent to an unsatisfactory extent.

Platzman et al. (1981) list a number of areas for further investigation. This work will address some of those areas, such as higher resolution of the bathymetry, inclusion of self–attraction and loading, the role of the Arctic Ocean, and systematic testing by means of diagnostic models. The effects of bathymetry definition are studied by comparing results obtained with grids of 4– and 2–degree resolution; these grids are defined in spherical coordinates. The role of the Arctic Ocean is determined by comparing results obtained with two 4–degree grids, one of which does not include the Arctic. Self–attraction and loading are modeled by the approximate method of Accad and Pekeris (1978). The Proudman method allows for variation in the number of eigenfunctions that are included in the Laplace tidal equation. These effects are studied by producing four solutions with the 4–degree grid, corresponding to the inclusion of 100, 500, 800, and 1500 eigenfunctions for each of the Stokes potentials.

The objective of this investigation is not to provide the final solution to the normal mode problem, rather it aims to show that the present state of the art is that such a solution still lies in the future. It is hoped that the various numerical experiments will exhibit where some of the difficulties lie, as well as provide some insight as to how to proceed in the future. If nothing else, the results should show that the normal mode periods obtained from present numerical models are still tentative and do not enjoy the same degree of accuracy as other physical constants, such as the gravitational constant or the velocity of light.

MATHEMATICAL PRELIMINARIES

The theoretical foundation of this method was developed by Proudman (1917); this investigation used a reformulation developed by Rao (1966). The theory provides the formalism for calculation of the gravitational and rotational normal modes of irregularly shaped basins with realistic bathymetry. The detailed mathematical formulation of the method can be found in Rao (1966). The present application to a world ocean model which includes islands requires the modification and extension of the methodology for it to be consistent with the topological configuration, specifically the solution of the stream function eigenvalue problem requires the reformulation of the boundary conditions. The operator for the stream function eigenvalue problem is derived from the vorticity of the transport field,

$$\nabla h^{-1} \nabla \psi = -\mu \psi \qquad (1)$$

$\psi = o$ on main boundary

h: basin depth

μ: eigenvalue

ψ: eigenfunction

The impermeability of the boundary requires it to provide a contour of constant value for the stream function. The value is arbitrarily selected to be equal to zero in the simply connected problem. In a multiply connected domain, the boundary of the "mainland" can still represent a constant contour with zero value for the stream function, but the island boundaries represent contours of constant stream function value which differ from zero and these values have to be determined by means of line integrals around each of the islands. This problem was addressed originally by Kamenkovich (1961) in the context of wind–driven ocean circulation problems and more recently, by Platzman (1979) with application to the normal mode problem. Platzman (private communication) provided the boundary conditions to be used specifically in the solution of the stream function eigenvalue problem

$$\oint_{c_j} h^{-1} \frac{\partial \psi}{\partial n} \, ds = o$$

$\psi = b_j$

c_j: boundary of island "j"

b_j: constant to be determined

These boundary conditions can be obtained from considerations of single–value for the surface displacement, but they also follow naturally from the self–adjointness requirement for the operator. The eigenvalue problem for the velocity potential requires no modification in the multiply connected case; the divergence of the transport field and boundary impermeability yield

$$\nabla h \nabla\phi = -\lambda \phi$$
$$h \frac{\partial \phi}{\partial n} = 0, \text{ on boundaries} \qquad (2)$$

λ: eigenvalue
ϕ: eigenfunction

The substitution of the Proudman functions into the unforced Laplace tidal equations yields the third eigenvalue problem, the solution of which constitutes the main goal of this investigation:

$$(\sigma \underline{\Pi} - i \underline{M}) \underline{S} = 0 \qquad (3)$$

σ: eigenvalues of matrix $i \underline{M}$
$\underline{\Pi}$: identity matrix
$\underline{S}$: matrix with eigenvector columns of expansion coefficients
$\underline{M}$: matrix formed from Laplace tidal equations
$i = \sqrt{-1}$

COMPUTATIONAL PRELIMINARIES

I.) The Grids

The numerical images of the operators appearing in equations (1) and (2) were obtained using finite differences. The finite difference equations were obtained by means of three different grids, all of them expressed in spherical coordinates. The angular distance between adjacent velocity potential points or between adjacent stream–function points is 4 degrees for two of the grids—one with and one without the Arctic. The third grid has a 2–degree definition and includes the Arctic. Figure 1 shows the grids and Table 1 gives pertinent information. Grids A4 and A2 do not include the Arctic in its totality; a small cap covers the North Pole and connects with Greenland. To that extent, any Arctic modes produced by the models will be unrealistic, hopefully, the effect produced by the inclusion of the Arctic approximation on the global model will still be realistic. The presence of a small cap at the North Pole simplifies the computer coding. The bathymetry data used in each of the grids were obtained from the 5' database of the World Data Center in Boulder, Colorado, with 2– and 1–degree averages for the 4– and 2–degree grids, respectively.

II.) The Lanczos Method

The Lanczos technique was used to formulate the matrix image of the operator appearing in the stream–function problem. The iterative nature of this method makes it convenient to deal with the line integral appearing in the boundary conditions.

The Lanczos method was used also in the formulation of the velocity potential problem in the 2–degree grid. In all cases, renormalization was implemented in the creation of the Lanczos basis—for the 2x2 model, this means 9608 iterations for the velocity potential, and 8869 iterations for the stream function, with every Lanczos auxiliary vector being normalized with respect to the previous one. Various eigensystem analysis subroutines from the IMSL/MATH LIBRARY were used to solve the matrix–eigenvalue problems, and the subroutines BISECT and TINVIT from EISPACK were used with the Lanczos method. The hardware consisted of CRAY computers available at the Goddard Space Flight Center and at Cray Research, Inc., in Minneapolis. For more details, see Morrow and Sanchez (1992).

III. The Normal Modes Matrix

It can be shown that if (n) velocity potential eigenfunctions and (n) stream–function eigenfunctions are substituted into the Laplace tidal equations (L.T.E.) the matrix $\underline{M}$ will have size (3n x 3n). The solution eigenvalues appear as a column of length 3n, the midpoint separates two mirror images with opposite signs. The two signs for every eigenvalue correspond to opposite senses of phase propagation for every mode. Every set of (3n/2) distinct eigenvalues is composed of (n/2) values that correspond to rotational modes modified by gravity and (n) values associated with gravitational modes modified by rotation. As is well known, the gravitational modes have a limit point at infinite frequency, the rotational modes have a limit point at zero frequency, and the wavelength approaches zero at each. The matrix of solution eigenvectors $\underline{S}$ is partitioned in a similar manner, two submatrices of size (3n/2) x (3n) appear, mirror images of each other. In the absence of friction, the matrix i $\underline{M}$ is hermitean, its eigenvalues are real and its eigenvectors are orthogonal.

The structure of the matrix $\underline{M}$ allows the identification of the rotational modes modified by gravity and the gravitational modes modified by rotation, as they appear in the solution matrix $\underline{S}$. The energy of the rotational modes is mostly kinetic, while the gravitational modes are characterized by approximate equipartition between kinetic and potential. The exception to this rule occurs at the boundary between the two types of modes. In this area, some of the modes in the gravitational regime have large values of kinetic energy and show space structures characteristic of vorticity modes. However, it is still possible to associate zero–rotation periods with these modes; therefore, they are included in the gravity mode spectrum in this report. The zero–rotation period is the normal mode period obtained when the Coriolis parameter vanishes.

NUMERICAL RESULTS

I.) Results Using the 4–Degree–Resolution Grids

a.) The number of Proudman functions included in L.T.E.

As seen in Table 1, computations using the 4–degree grids involve approximately one–fourth the number of degrees of freedom of the 2–degree case. Many areas of investigation can be addressed with the 4–degree grids at great savings of computational effort. One such area involves the behavior of the normal mode solution as a function of the number of Proudman functions inserted into the L.T.E., for that purpose, four solutions were generated using grid A4. The number of functions of each type used in the L.T.E. being 100, 500, 800, and 1500, respectively. The results are displayed in Table 2, and in Figures 2 and 3. Table 2 shows the periods of selected gravity modes for the four cases. Figure 2 shows the first 50 periods (gravity modes) for the four solutions. The inclusion of more eigenvectors in the solution yields more modes at the faster end of the spectrum, as is to be expected from wavelength considerations. Figure 3 shows the periods for the fastest 50 rotational modes for each of the four cases, with the exception of the 100–function case, which includes only the fastest 25 modes. The four solutions are certainly quite apart, the inclusion of more eigenvectors maps into a decrease in the periods of the rotational normal modes.

b.) The Arctic Ocean

In order to ascertain the effect of the Arctic Ocean, a solution with grid NA4 was computed with 500 eigenvectors of each type inserted into the L.T.E. Figure 4 shows the periods of the 50 slowest gravity modes for this solution and for its counterpart (500 functions), which includes the Arctic. Figure 4 shows longer periods for the model that includes the Arctic; this does not mean that each mode had its period lengthened, but that the entire spectrum has shifted due to the presence of the new modes, as shown in Table 3.

To determine the effect of the Arctic Ocean on a particular mode, Table 4 should be considered, which shows the normal mode periods for three of the models, as well as the potential energy percentage of total energy and the zero–rotation period (when applicable), for the range 50–90 hours. The modes with no zero–rotation period are rotational modes modified by gravity. The first gravity modes modified by rotation have periods of 62.8 hours for the 4° x 4° model with no Arctic, 76.4 hours for the 4° x 4° model with the Arctic, and 71.9 hours for the 2° x 2° model. These modes have relatively low levels of potential energy (their space structures are shown in Figure 7) and they are essentially vorticity modes, as pointed out by Platzman *et al.* (1981).

The first gravity modes for the three models have periods of 50.4, 54.8, and 66.9 hours. The space structures for the first two are shown in Figure 8. The results for the two 4° x 4° grids indicate that the inclusion of the Arctic Ocean produces an increase in the normal mode periods. This increase is 4.4 hours for the first legitimate gravity mode and 13.6 hours for the vorticity mode.

c.) Loading and Self–attraction

The effects of loading and self–attraction have been simulated by an approximate approach, originally due to Accad and Pekeris (1978), and also used by Schwiderski (1980) in the context of computation of the forced solutions to the L.T.E.

$\hat{\zeta} = 0.10\zeta$

ζ: surface displacement

$\hat{\zeta}$: additive effect due to self–attraction and loading

A more exact representation requires theoretical developments in terms of the Proudman function basis, which are not available at the present time; the existing theory being in terms of spherical harmonics. Figure 5 shows the results for the loading and self–attraction solution, and for the standard case without it. Loading and self–attraction lengthen the periods slightly, as was predicted by Marchuk and Kagan (1989), from Rayleigh's ratio analysis.

d.) Space Structure of the Modes

Every mode has a space–dependent amplitude and phase distribution. A comprehensive atlas of such distribution for each mode is beyond the scope of this presentation. Instead, specific geographic areas will be analyzed in terms of the 50 slowest gravity modes and plots of amplitude and phase for a few specific modes will be given. The mean–square elevation of a mode is given by,

$$\overline{\zeta^2} = \int \zeta^2 \, da/A$$

$\overline{\zeta^2}$: mean-square elevation

A: oceans' area

The normalized regional mean–square elevation is given by,

$\overline{\zeta_i^2}/\overline{\zeta^2}$

$\overline{\zeta_i^2}$: regional mean–square elevation.

A mode of uniform amplitude will have a value of 1 for its normalized regional mean–square elevation in all regions, non–uniform amplitude distributions will have a value greater than 1 for energetic regions, and less than 1 for "quiet" areas. A value of 1 indicates average activity, not necessarily uniform amplitude.

Figure 6 shows the distribution of normalized regional mean–square elevation for the 50 slowest gravity modes as computed using grid NA4, which excludes the Arctic Ocean. The bottom panel shows the results obtained for a region defined by a cap on the South Pole, which extends 10 degrees north of the Antarctic Circle, to colatitude 146.5 degrees. This region has been chosen in order to search for modes which might be associated with Kelvin waves around Antarctica. Such a mode was obtained by Platzman (1981) in his calculations.

The most energetic mode in the Antarctic region is mode number 7, with a period of 29.59 hours. The amplitude and phase distributions for this mode are displayed in Figure 9, which shows the characteristics of an Antarctic Kelvin wave. Other peaks occur at mode number 23, with a period of 14.84 hours, and at mode number 48, with a period of 9.38 hours.

Figure 6 also presents the results of computations using grid A4, which includes the Arctic Ocean. The middle panel shows the results for an Antarctic cap as previously defined; the top displays the results for an Arctic cap defined by the Arctic Circle. Most of the modes are very energetic in the Arctic Ocean, the highest peak corresponding to mode number 47, with a period of 12.09 hours.

The Antarctic region has its peaks at mode 38, with a period of 14.63 hours, and mode 14, with a period of 29.44 hours. Figure 9 shows the amplitude and phase structure for mode 14—the Antarctic Kelvin wave is evident.

II.) RESULTS USING THE 2–DEGREE–RESOLUTION GRID

The grid A2 was used to compute Proudman functions, and 500 of each type were used in the normal mode solution.

The spectrum of gravity modes covers a period range from 71.9 hours to 3.54 hours. Figure 10 shows the periods for this solution and the periods obtained with grid A4. The curve for the 2–degree grid shows longer periods, but this is produced by a shift due to the greater number of modes in the 10– to 80–hour range (see Table 3). The period of the gravest mode has decreased however, from 76.4 to 71.9 hours. The corresponding curves for the periods of the vorticity modes are shown in Figure 11; the 2–degree solution now shows faster periods than its coarser counterpart, but again, identical mode numbers do not necessarily refer to the same physical mode structure. The periods of the rotational modes

range from 83.87 hours to 15.82 years. The effects of self–attraction and loading were modeled by the same approximate technique used in the 4–degree case; the results are given in Table 5. On the average, self–attraction and loading lengthens the periods by about 5 to 6 percent. Normalized computations were performed using polar caps as defined in the 4–degree grids. The results are displayed in Figure 12. For the 300 slowest gravity modes, note that mean elevation is now plotted as a function of period. Many modes are energetic in the Arctic Ocean (top panel of the figure). There are 106 modes with normalized elevation values between 1 and 10, 38 between 10 and 20, 57 between 20 and 30, and 21 greater than 30.

The Antarctic region has 26 modes with elevation values between 1 and 2, and 3 modes with values between 2 and 3. There are peaks for modes with periods of 30.57, 28.92, 28.40, and 27.99 hours; these correspond to fundamental Kelvin waves around Antarctica. Peaks at 15.74 and 14.71 hours can be identified with the second harmonics. Higher wave numbers are present at a number of modes with periods in the 5– to 11–hour range. Amplitude and phase for some of the modes are given in Figures 13–17. Note the amphidrome in the North Sea, which clearly appears in some of the modes, but that the 4–degree grid resolution was unable to reproduce.

SUMMARY

Table 5 gives a summary of the first 20 gravity modes obtained in the various experiments.

It was found that the number of Proudman functions included in the Laplace tidal equations (after an initial minimum) does not produce great changes in the periods and structures of the gravity modes (with the exception of the slowest two modes, which are essentially vorticity modes).

The addition of more eigenfunctions fills the short–wavelength part of the spectrum, and faster modes are obtained, which were not present before. The results for the vorticity modes indicate that the addition of more functions produces large changes in the periods throughout the spectrum—the changes being larger as the periods get larger and the wavelengths become smaller. As more functions are included, the entire spectrum become faster. If proper numerical controls are maintained, the solution with more functions should be more accurate, however, the size of the matrix could be a constraining factor. The inclusion of the Arctic Ocean can produce changes in the periods and structures of the modes, especially in the regions closer to the Arctic, as expected. New modes appear in the solution, and many are quite energetic in the Arctic. The period of the slowest gravity mode is lengthened by almost 4.4 hours by inclusion of the Arctic Ocean.

The effects of loading and self–attraction were simulated by the approximate method of Accad and Pekeris; the periods of the gravity modes were lengthened by less than 10 percent. Computations using a finer grid with 2–degree resolution result in a greater number of modes appearing in the long–wavelength part of the gravity mode spectrum.

A comparison of the solutions in the rotational mode band shows similarity in the shape of the periodicity curve, with the 2–degree solution having faster periods than the 4–degree case.

Figure 18 shows the modal periods in the diurnal and semidiurnal spectral bands, as obtained by different investigations; it is a reproduction of Table 4.3 by Marchuk and Kagan (1989), but it has been extended to include the results of this investigation. Various methods were used by the different investigations. The grid resolution also varies: Protasov, and Gotlib and Kagan used 5–degree finite difference grids; Gaviño Rodriguez, a 4–degree grid; Platzman, a finite–element grid with an average area equal to a 4.54–degree equatorial square. The results for Sanchez and Morrow (4–degree grid with the Arctic) correspond to the case using 1500 eigenfunctions for each of the Helmholtz potentials.

It is not surprising that Figure 18 shows discrepancies in the spectrum obtained by the various investigations; there are differences in the grid resolution and method of solution, and also in the lateral boundaries of the domains—as shown in Figure 19. The computational bathymetries are very likely to be different; this is also true for the various models used in this work, as shown in Table 1.

The results indicate that future numerical models should use grids of finer resolution and should include the Arctic Ocean. If the Proudman method is used, the solution should include as many Proudman functions as possible—especially if accurate resolution of the vorticity modes is desired. For more accuracy in the gravity mode calculation, self–attraction and loading should be included.

A few simplified models of friction were tried in this investigation, but the results were not deemed sufficiently important to be reported; the topic deserves a more careful and complete treatment. The numerical modeling of oceanic normal modes continues to suffer from lack of constraints as a result of lack of direct observations. Luther (1983) addressed this point in an excellent manner.

A more recent treatment by Platzman (1991) illustrates possible approaches for future analysis of oceanic data.

ACKNOWLEDGEMENTS

We express our appreciation to Richard Ray of Hughes STX Corporation, for the creation of the figures and plots appearing in the text. We would also like to thank Shannell Frazier of the Goddard Space Flight Center for her assistance, as well as Luann Bindschadler of the Technical Information Services Branch for her invaluable editorial work. We give thanks to William Cunningham of Hughes STX Corporation, for helping with some of the software problems. We acknowledge the support provided by the Space Geodesy Branch, GSFC, the TOPEX/ Poseidon project, and Cray Research, Inc. Last but not least, we give thanks to Professor G.W. Platzman, University of Chicago, for reading the manuscript and providing constructive criticism.

REFERENCES

Accad, Y., and Pekeris, C.L. 1978. Solution of the tidal equations for the M_2 and S_2 tides in the world oceans from a knowledge of the tidal potential alone. Phil. Trans. Roy. Soc. London, A290, 235-266.

Gotlib, V.Y. and Kagan, B.A., 1981. On the resonance excitation of semidurnal tides in the world ocean, Izv. AN SSSR. Fizika atmosfery i okeana, 17, 502-512.

Kamenkovich, V.M., 1961. The integration of the marine current theory equations in multiply connected regions. Dokl. Acad. Scci. U.S.S.R., 138, 629-631.

Luther, D.S., 1983. Why haven't you seen an ocean mode lately? Ocean Modelling, 50, 1-14.

Marchuk, G.I., and Kagan, B.A., 1989. Dynamics of ocean tides, Kluwer Academic Publishers, Boston.

Morrow, D., and Sanchez, B. 1992. Vector parallel speedup of a global ocean model. Proceedings of 30th Cray Users Group Meeting: Grand Challenges, Washington DC, Sept. 14, 1992.

Platzman, G.W. 1979. Effects of multiple connectivity on a finite-element barotropic model. J. Phys. Oceanogr., 9, 1276-1283.

Platzman, G.W., Curtis G.A., Hansen K.S. and Slater R.D., 1981. Normal modes of the world ocean. Part II: description of modes in the period range 8 to 80 hours. J. Phys. Oceanogr., 11, 579-603.

Platzman, G.W., 1991. Tidal evidence for ocean normal modes. Tidal Hydrodynamics, edited by Bruce B. Parker. John Wiley and Sons, Inc., New York.

Protasov, A.V. 1979. Numerical method of solving the problem of free oscillations in the world ocean in barotropic approximation. Meteorologiya i gidrologiya, 6, 57-66.

Proudman, J., 1917. On the dynamical equations of the tides, I, II, III. Proc. London Math. Soc., 18, 1-68.

Rao, D.B., 1966. Free gravitational oscillations in rotating rectangular basins. J. Fluid Mechanics, 25.

Rodriguez, J.H.G., 1984. On calculation of resonance oscillations of a world ocean's finite-difference model by means of the Lanczos method. Mitteilungen des Instituts Fur Meeresbunde der Universitat Hamburg. Nr. 27. Hamburg.

Schwiderski, E.W., 1980. On charting global ocean tides. Reviews of Geophysics and Space Physics, 18, 243-268.

Table 1. Grids used in the calculations

Grid	Angular definition	No. of basin points ϕ	No. of basin points ψ	Area 10^6 km^2	Mean Depth m	Maximum N. latitude	Arctic
NA4	$4° \times 4°$	2094	1849	326.1	4114	67.2°	No
A4	$4° \times 4°$	2306	1991	335.5	4028	84.0°	Yes
A2	$2° \times 2°$	9608	8869	342.1	3964	86.25°	Yes

Table 2. Gravity-mode periods (hours) of selected modes

Mode Number	No. functions included in L.T.E. 100	500	800	1500
1	79.0	76.4	75.5	64.6
100	7.25	7.54	7.54	7.54
500		2.76	2.77	2.77
800			2.15	2.15
1500				1.54

Table 3. Number of gravity modes in given period ranges*

Period Range (h)	$4° \times 4°$ No Arctic	$4° \times 4°$ Arctic	$2° \times 2°$ Arctic
60–80	1	2	3
40–60	2	4	7
20–40	10	17	25
10–20	31	42	70
0–10	456	435	395

* All three solutions use 500 eigenfunctions.

Table 4. Modes (periods 50–90 h)

4° × 4° (NA)			4° × 4° (A)			2° × 2° (A)		
Period	PE (%)	P($f = 0$)	Period	PE (%)	P($f = 0$)	Period	PE (%)	P($f = 0$)
88.5	10.4		89.2	8.1		89.6	14.2	
77.2	22.4		76.4	23.6	127.2	83.8	38.4	
62.8	17.1	104.7	63.1	18.9	90.8	71.9	25.5	122.4
50.4	40.2	65.0	54.8	52.2	64.1	66.9	49.8	85.5
			53.3	54.8	50.0	61.9	64.9	66.9
						58.3	49.8	63.9
						52.9	58.2	57.9
						51.5	55.2	52.8

All cases: 500 eigenfunctions of each type, no loading.
PE (%): Potential energy percentage of total energy.
P($f = 0$): Period at zero rotation.
NA: No Arctic A: Arctic

Table 5. Gravity-mode periods (hours)

Mode	$4° \times 4°$ (A, NL)			$4° \times 4°$ (500)			$2° \times 2°$ (500)	
no.	100	800	1500	NA, NL	A, NL	A, L	A, NL	A, L
1	79.0	75.5	64.6	62.8	76.4	78.4	71.9	73.9
2	63.9	62.8	61.5	50.4	63.1	64.4	66.9	70.5
3	55.2	54.6	54.0	42.0	54.8	58.0	61.9	66.4
4	53.2	53.2	52.5	37.4	53.3	56.4	58.3	61.5
5	48.7	48.3	47.5	35.9	48.5	50.9	52.9	56.5
6	43.0	43.0	42.7	31.0	43.1	45.6	51.5	54.6
7	39.4	39.1	38.5	29.6	39.6	42.0	49.6	52.5
8	38.6	38.5	38.0	25.7	38.6	40.6	45.9	48.3
9	36.9	36.8	36.5	25.4	37.0	39.1	41.7	44.1
10	35.6	35.4	34.9	23.9	35.7	37.6	40.9	43.5
11	34.4	34.4	34.1	23.0	34.5	36.3	37.5	39.9
12	33.8	33.6	32.0	21.2	33.9	35.7	36.2	38.3
13	31.3	31.1	30.8	20.6	31.2	32.9	34.0	35.8
14	29.2	29.3	29.2	19.7	29.4	31.1	33.2	35.2
15	29.0	28.9	28.7	19.0	29.2	30.8	31.6	33.3
16	27.7	27.5	27.4	18.2	27.7	29.3	30.6	32.1
17	27.2	27.2	27.2	17.9	27.2	28.7	29.4	31.3
18	25.5	25.5	25.4	17.6	25.6	27.1	28.9	30.4
19	24.9	24.9	24.7	16.8	24.9	26.3	28.4	29.9
20	24.3	24.2	24.0	16.2	24.3	25.6	28.0	29.4

NA: No Arctic
NL: No Loading
A: Arctic
L: Loading
100, 500, 800, 1500: Number of eigenfunctions in solution
$4° \times 4°$, $2° \times 2°$: Grid definition

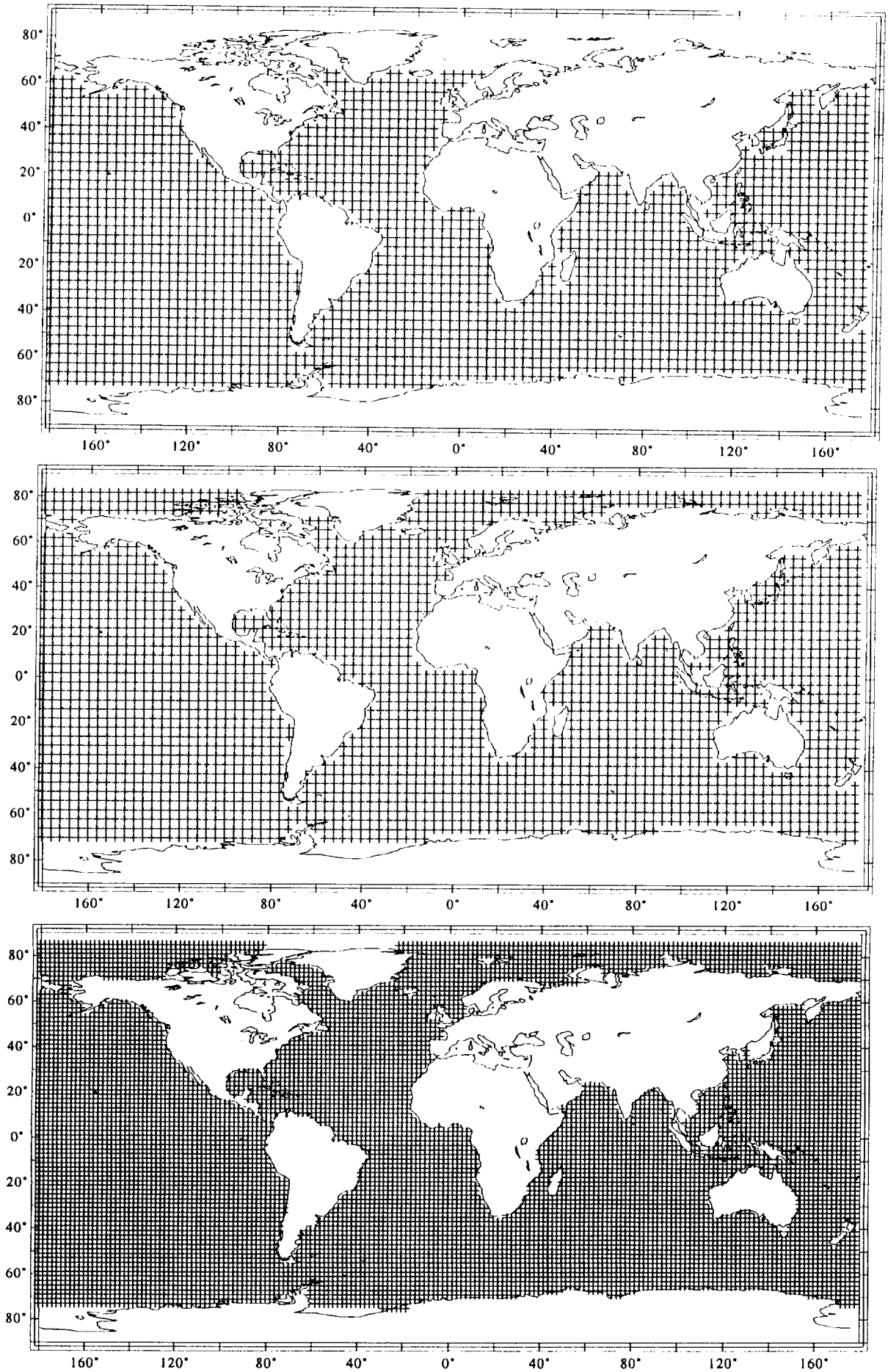

Figure 1. Spherical coordinates grids used in the computations. From top to bottom: 4 degree without the Arctic; 4 degree with the Arctic; and 2 degree with the Arctic.

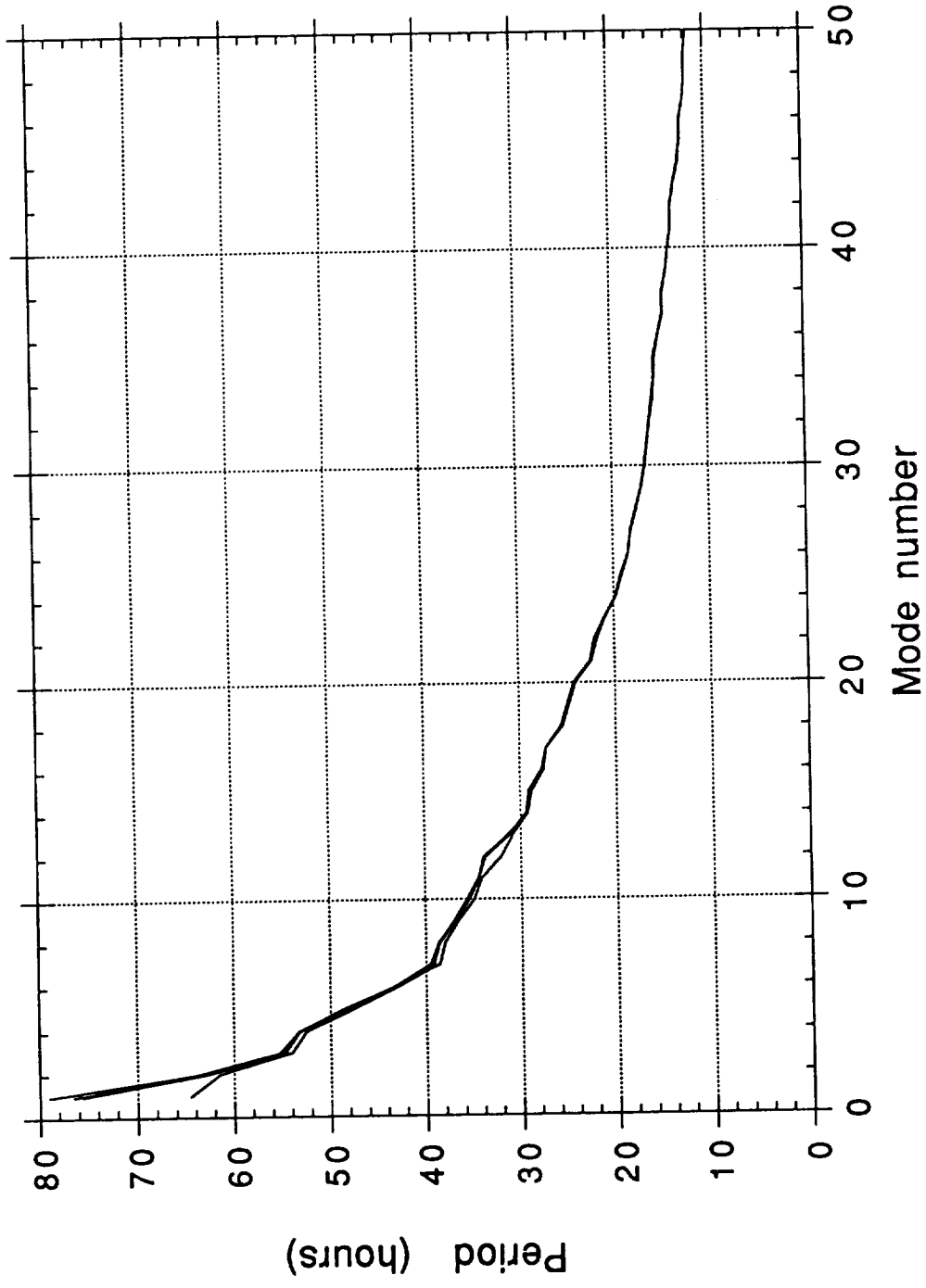

Figure 2. Periods of the gravity modes for the four solutions computed using the 4–degree grid with the Arctic.

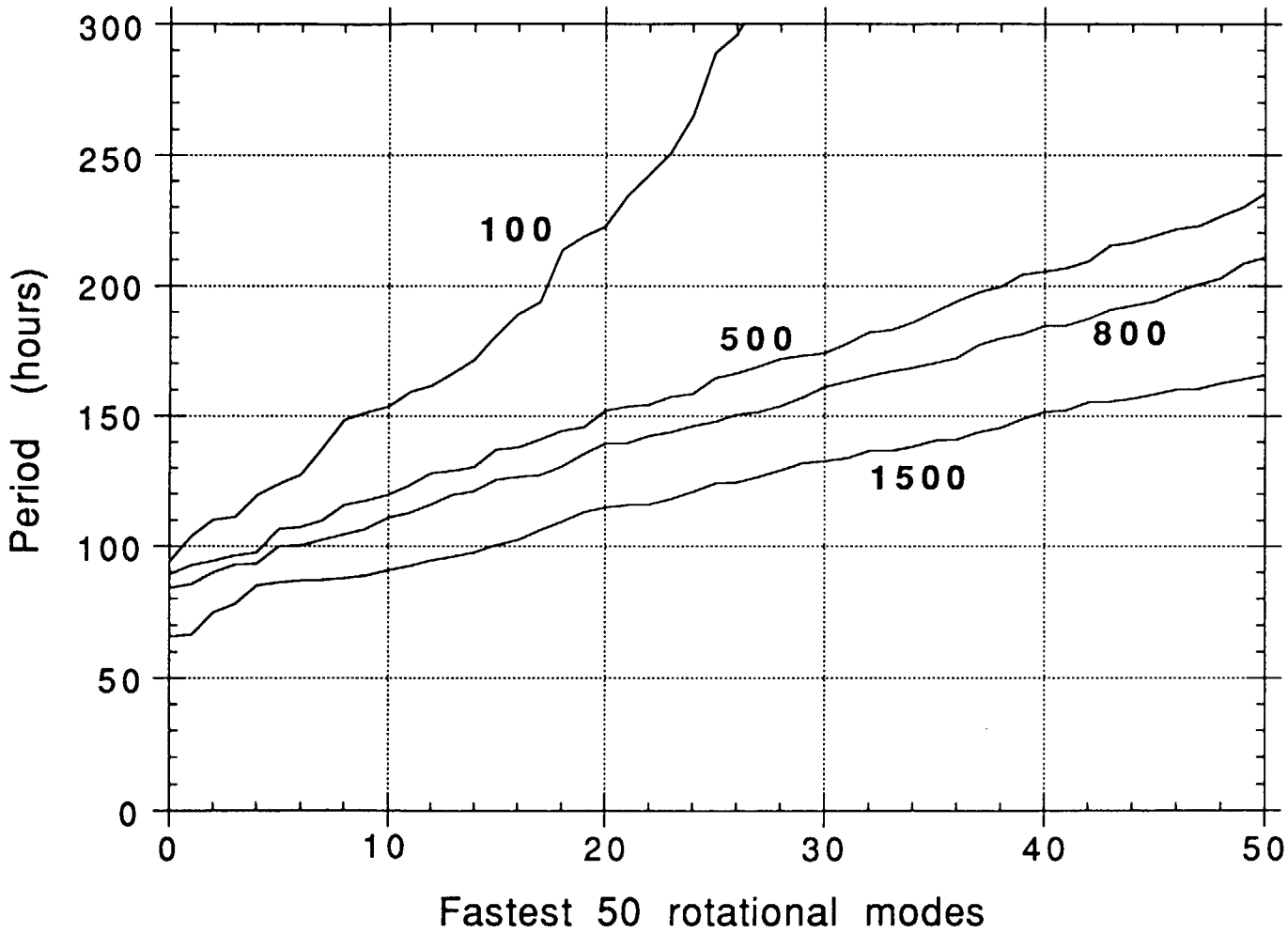

Figure 3. Periods of the rotational modes for the four solutions computed using the 4–degree grid with the Arctic.

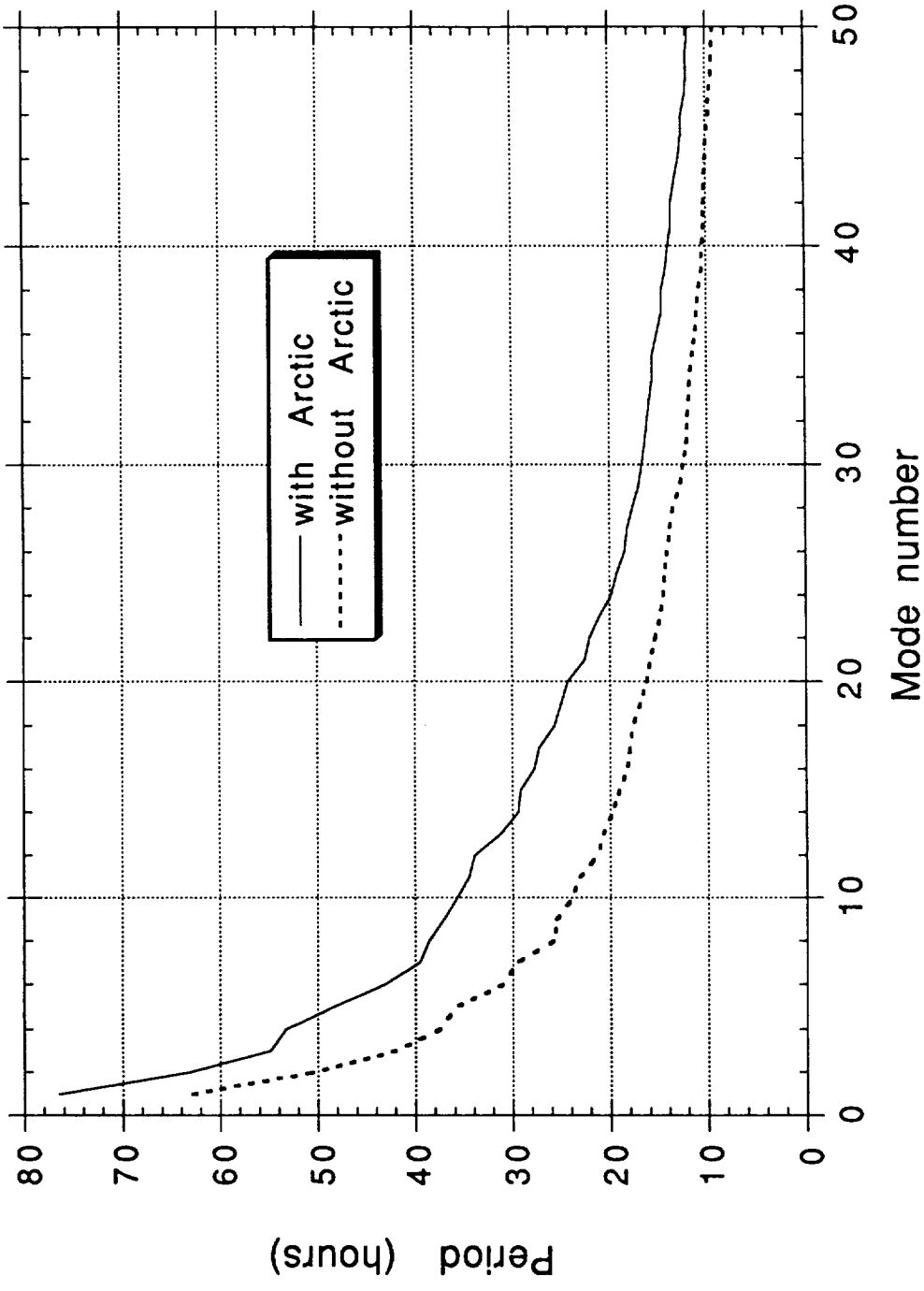

Figure 4. Periods of the gravity modes for the 4–degree solutions (500 functions), with and without the Arctic.

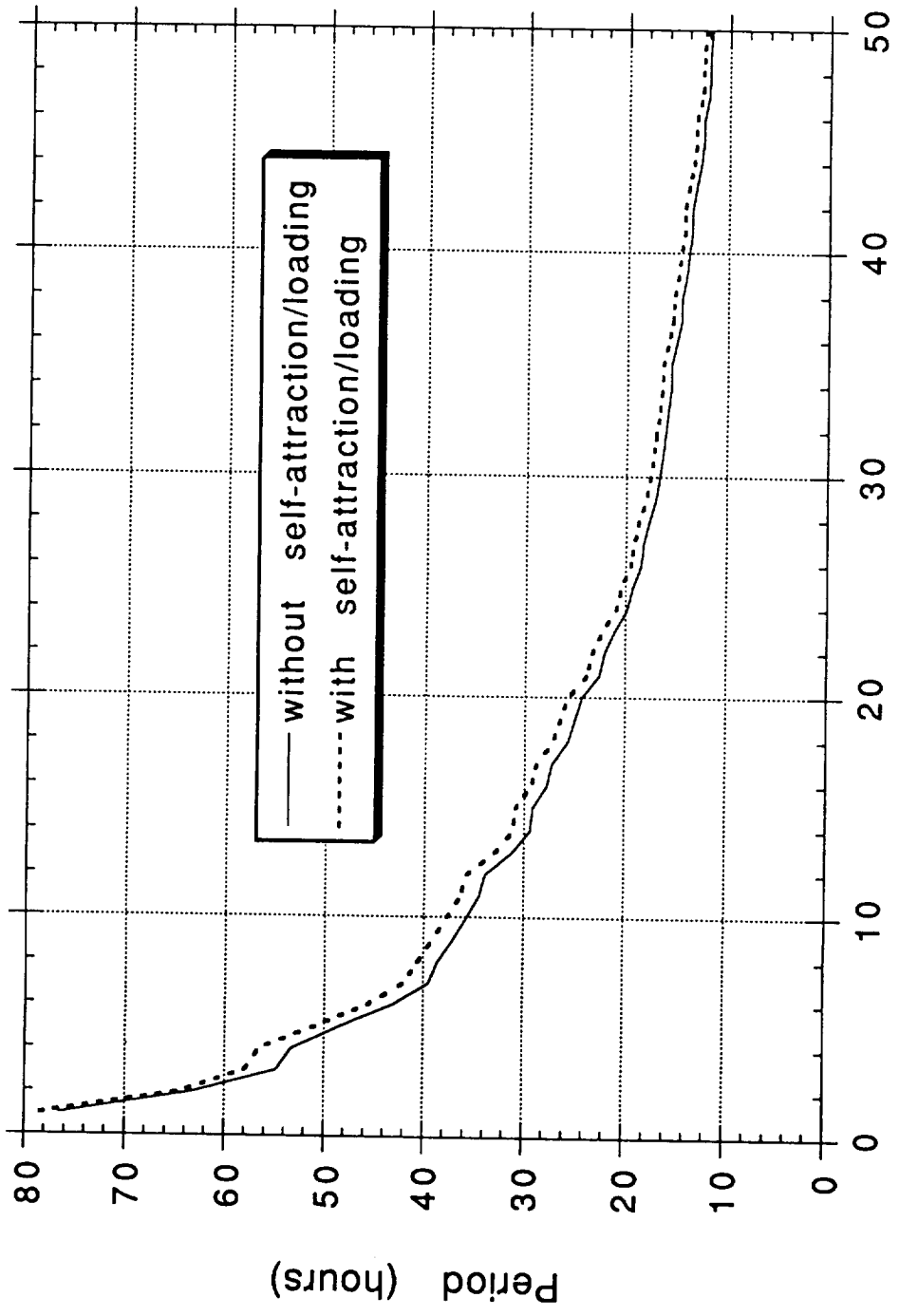

Figure 5. Periods of the gravity modes for the 4–degree solutions (500 functions), with and without self–attraction and loading.

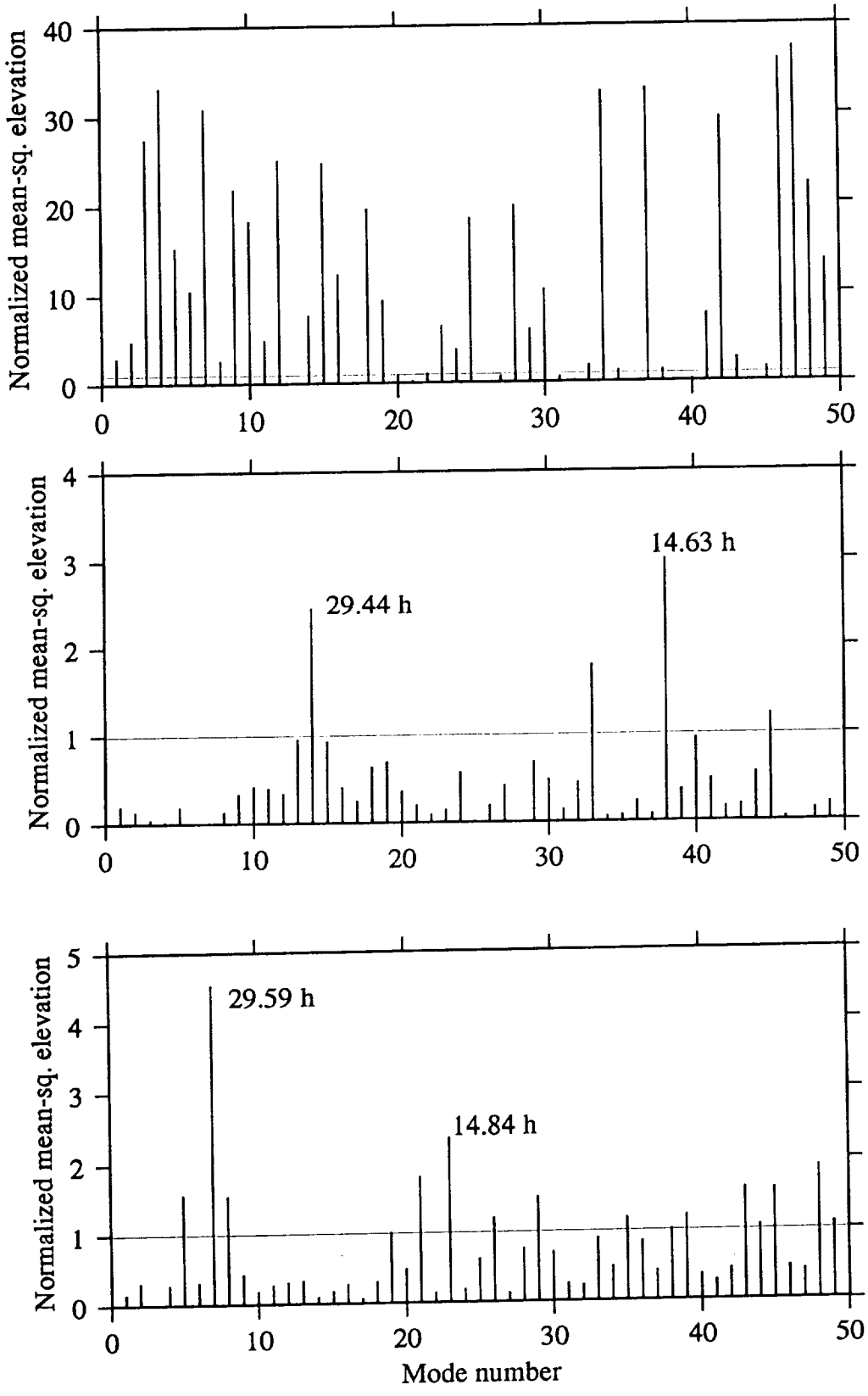

Figure 6. Normalized regional mean–square elevation for the slowest 50 gravity modes, 4–degree solutions. *Bottom panel*: ocean region defined by a South Pole cap extending to 10 degrees north of the Antarctic Circle. Solution with grid NA4 (no Arctic). *Middle panel:* ocean region as defined in bottom panel. Solution with grid A4 (Arctic included). *Top panel:* ocean region defined by a North Pole cap delimited by the Arctic Circle. Solution with grid A4.

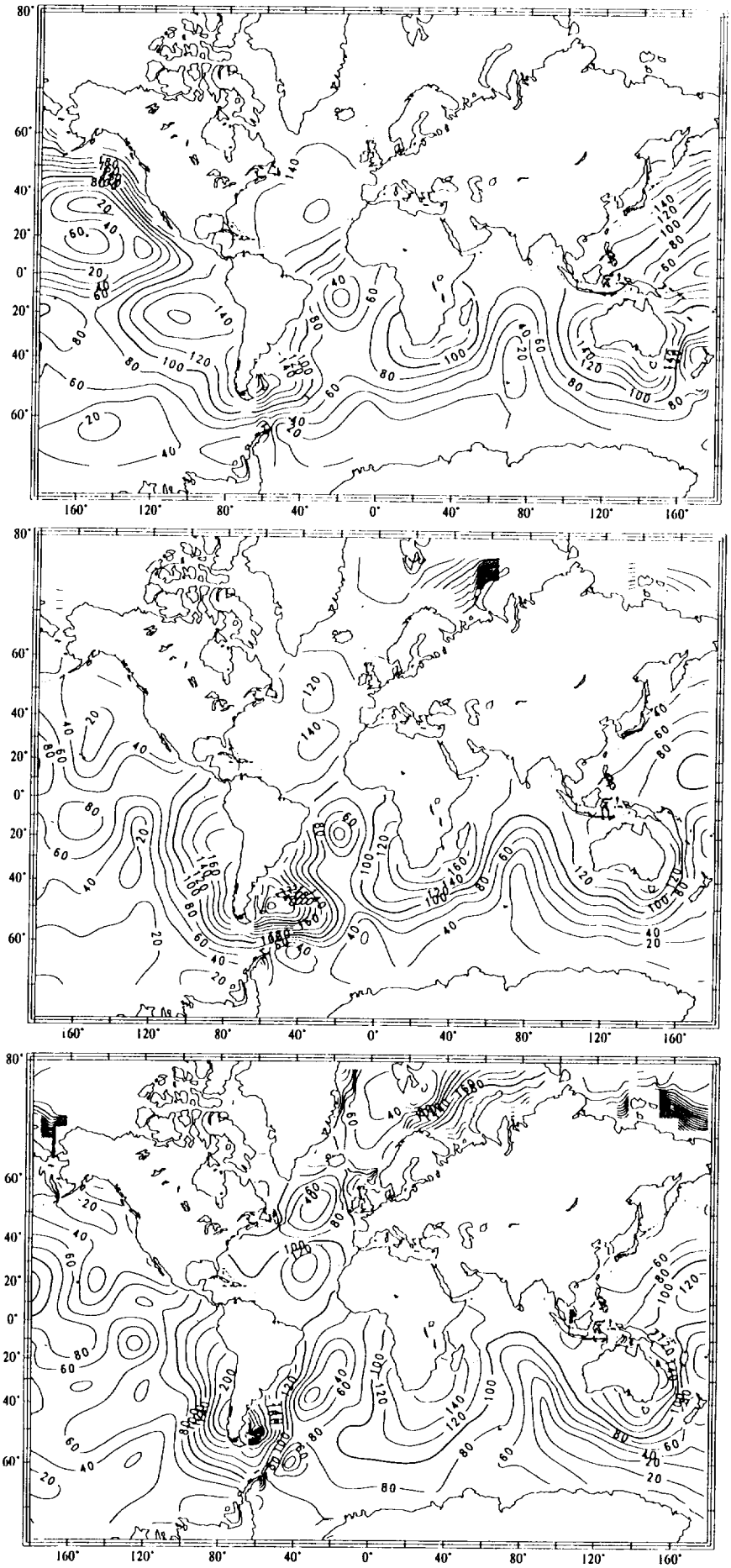

Figure 7A. Amplitude Contours. Amplitude normalized to RMS elevation equal to 100. Solutions: 500 functions, no loading and self–attraction. *Bottom panel:* mode with period of 71.9 hours, 2–degree solution. *Middle panel:* mode with period of 76.4 hours, solution with grid A4. *Top panel:* mode with period of 62.8 hours, solution with grid NA4.

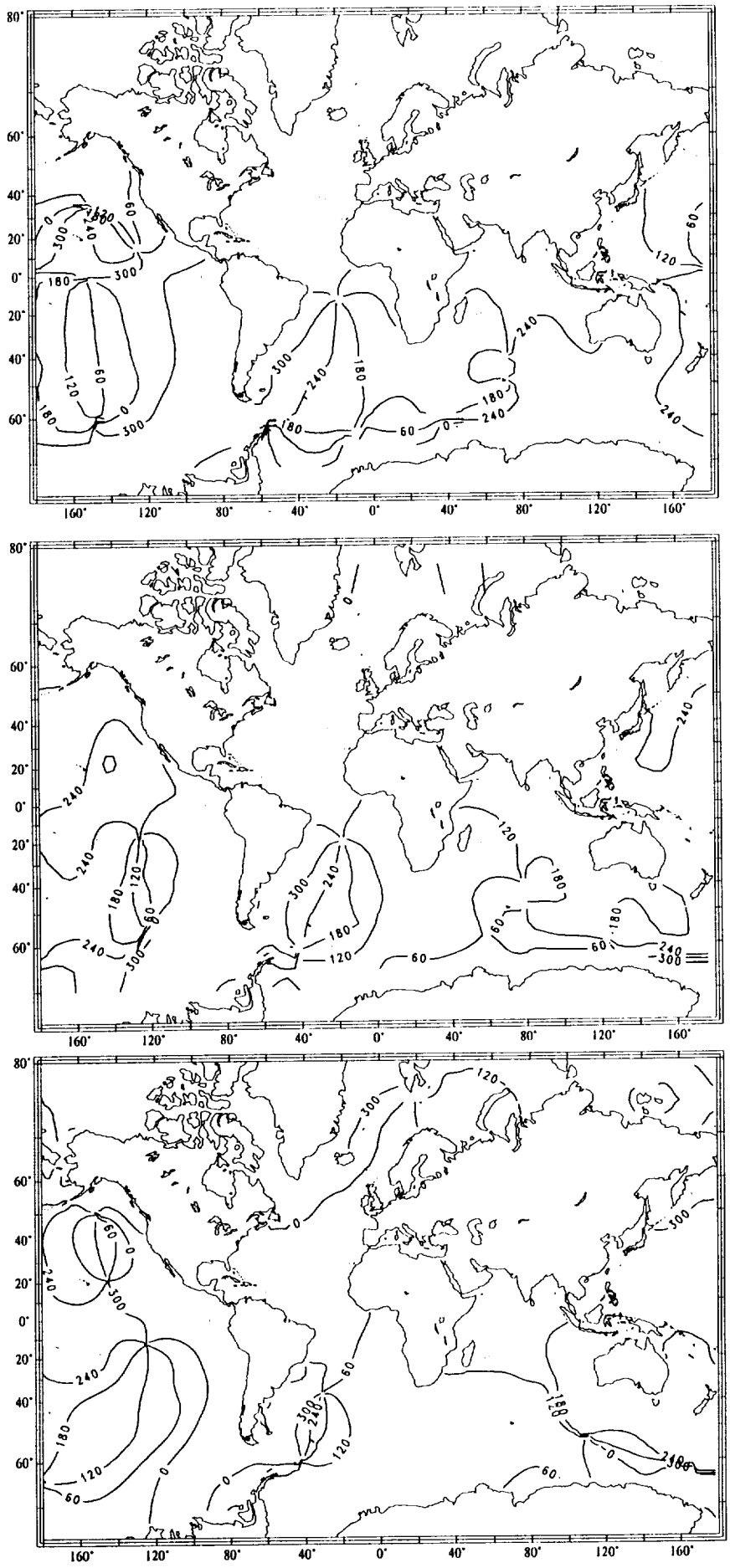

Figure 7B. Phase Contours. Zero phase is assigned to the grid point closest to the Strait of Gibraltar. Bottom, middle and top panels are as in Figure 7A.

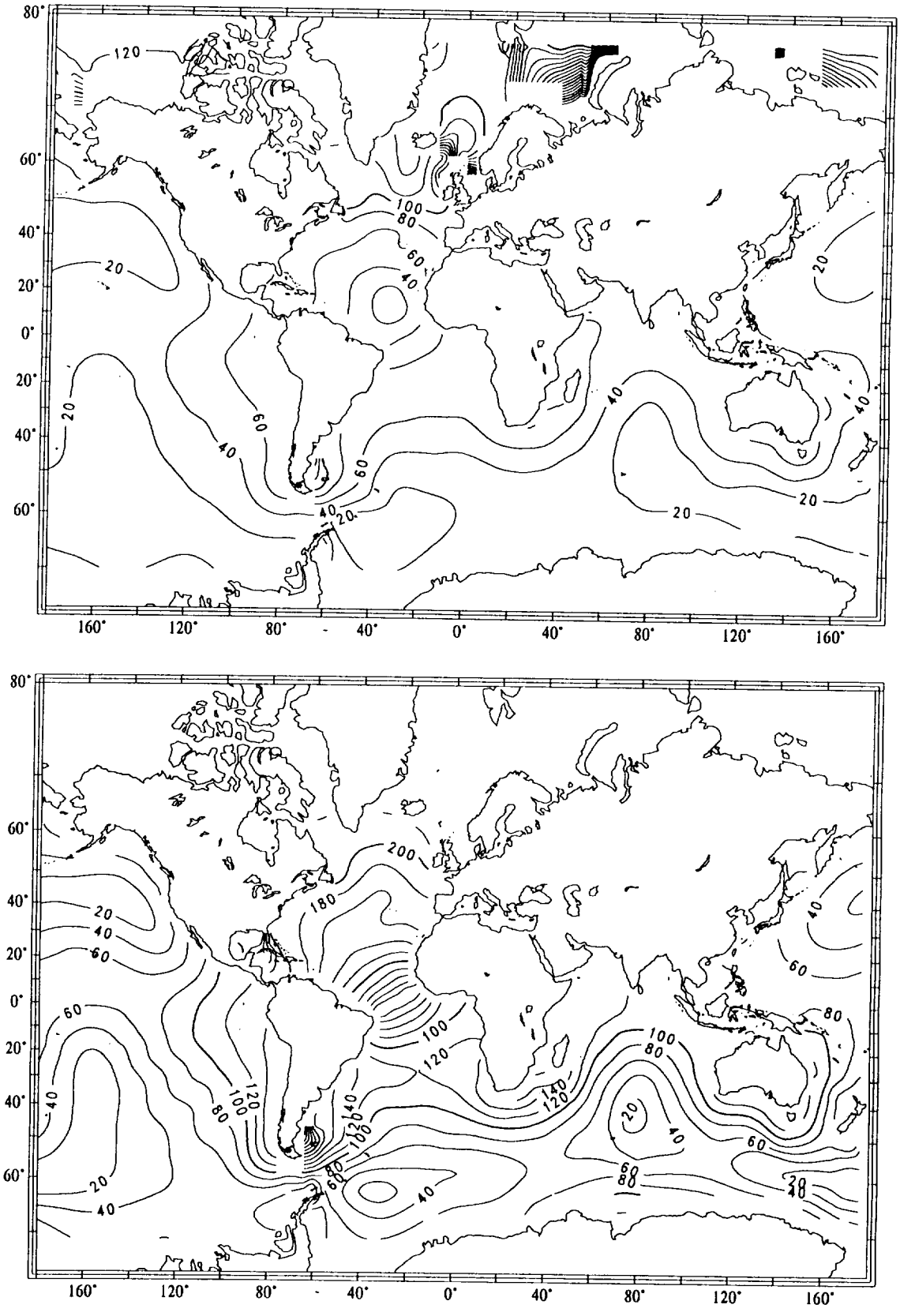

Figure 8A. Amplitude Contours. *Bottom panel:* mode with period of 50.4 hours, solution with grid NA4. *Top panel:* mode with period of 54.8 hours, solution with grid A4.

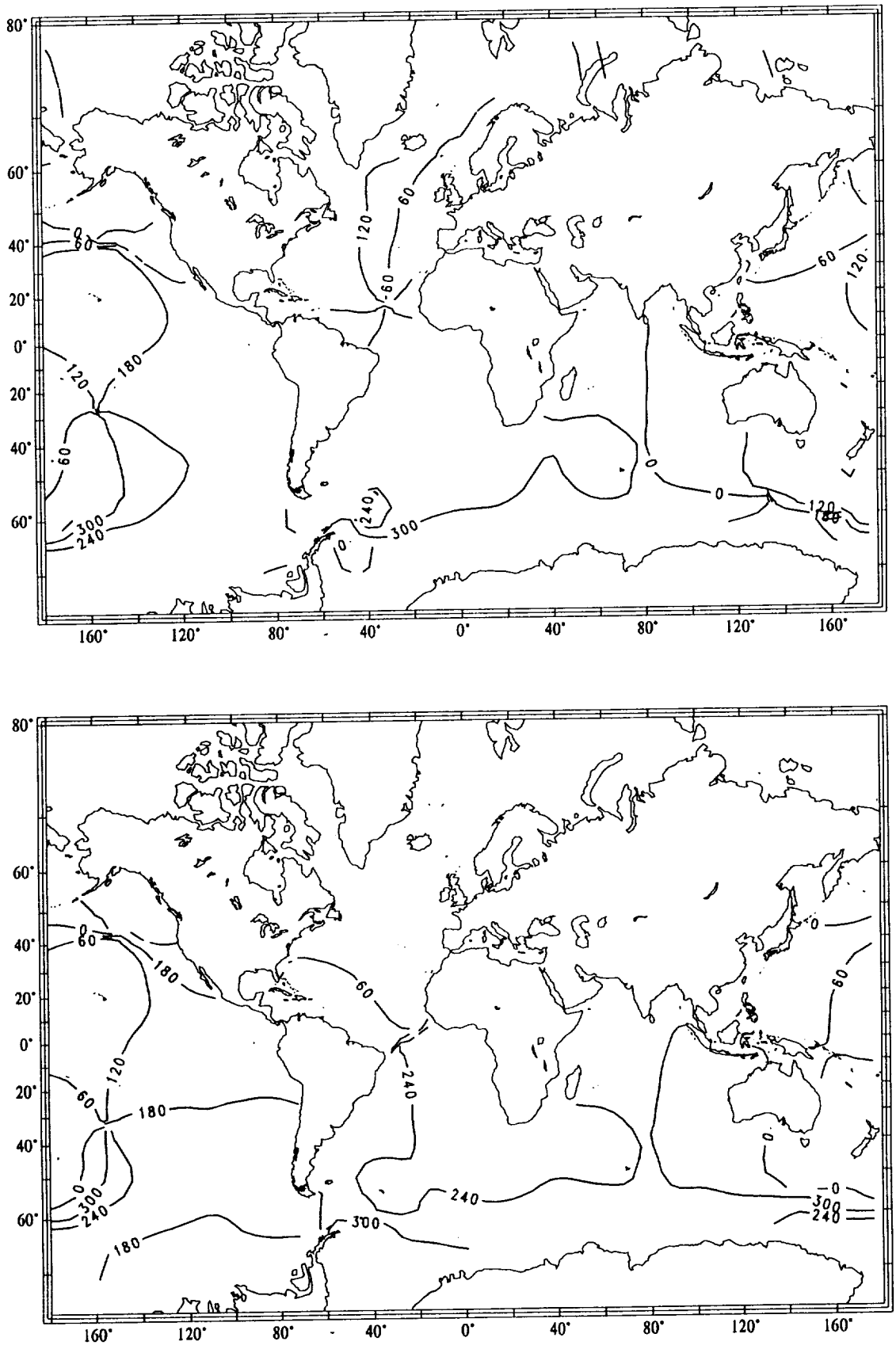

Figure 8B. Phase Contours. Bottom and top panels are as in Figure 8A.

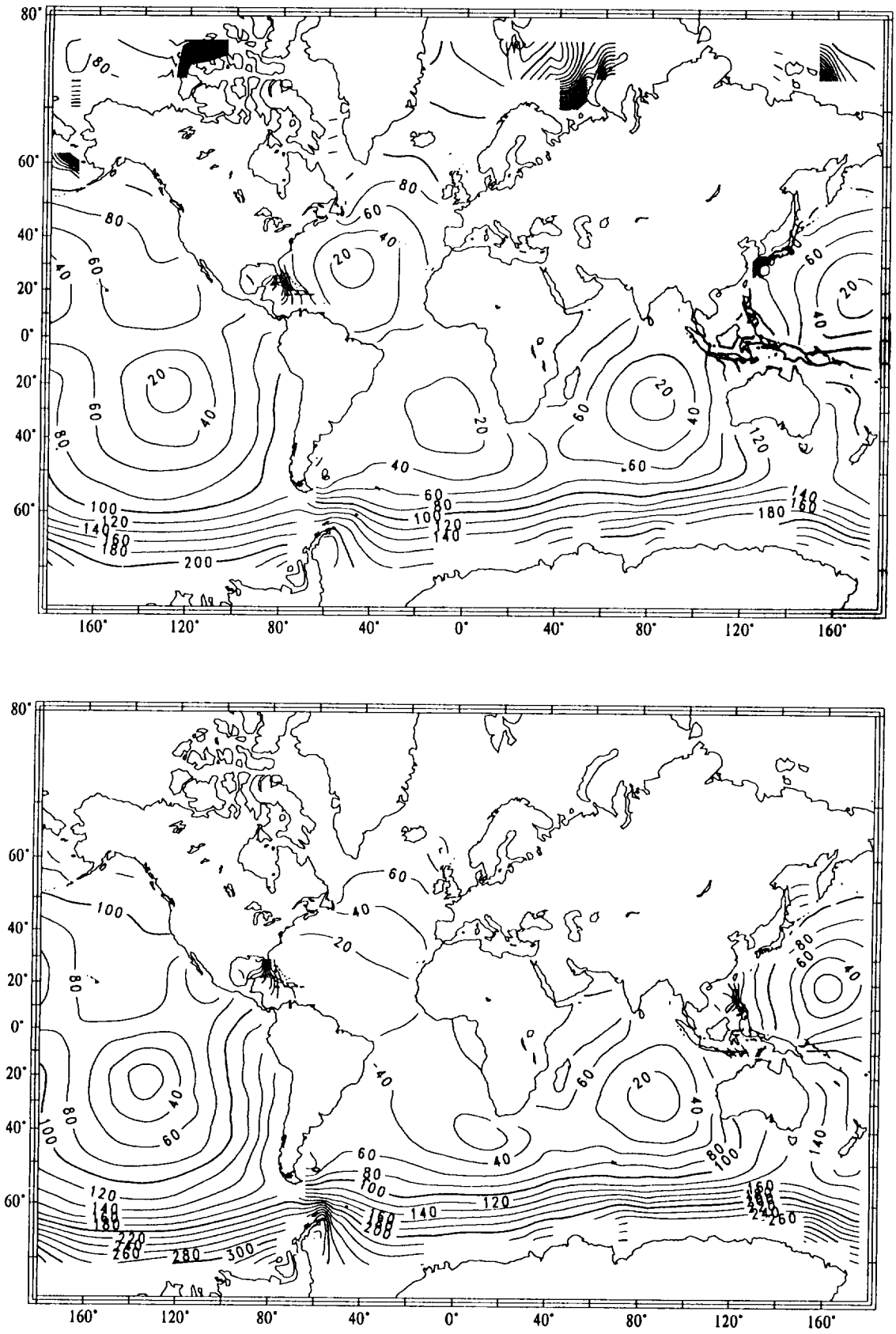

Figure 9A. Amplitude Contours. *Bottom panel:* mode with period of 29.59 hours, solution with grid NA4. *Top panel:* mode with period of 29.44 hours, solution with grid A4.

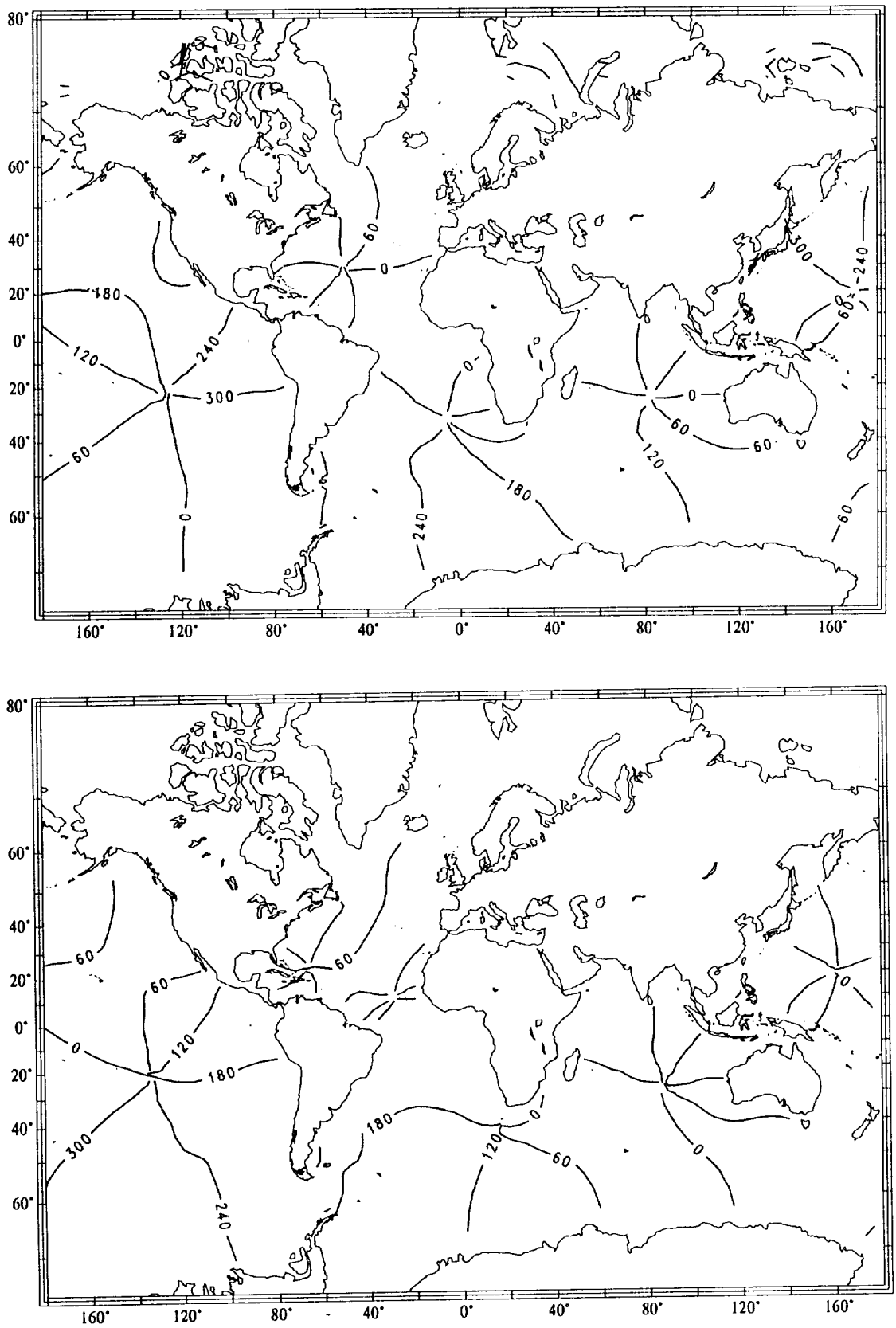

Figure 9B. Phase Contours. Bottom and top panels are as in Figure 9A.

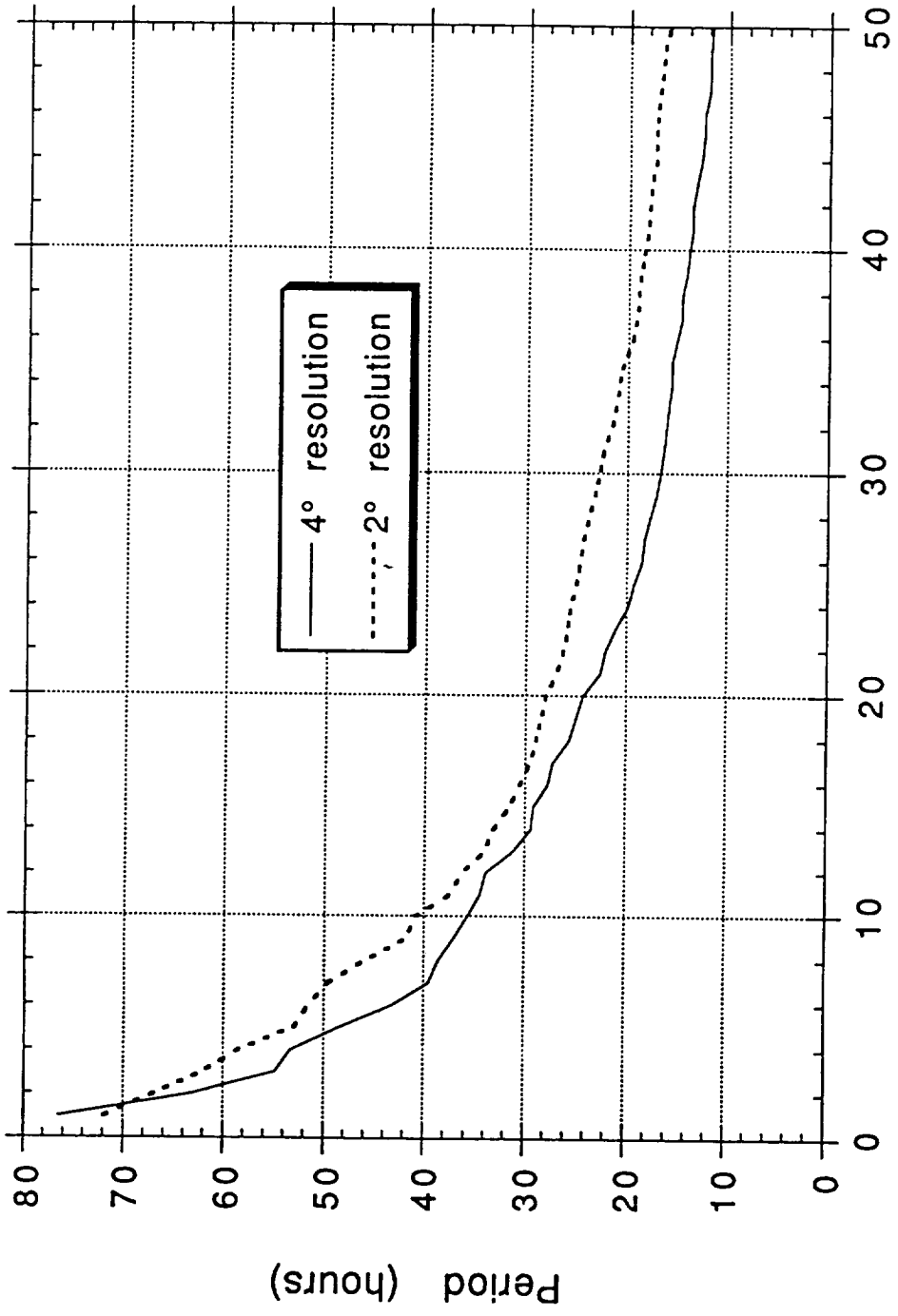

Figure 10. Periods of the gravity modes for the 2–degree and 4–degree solutions.

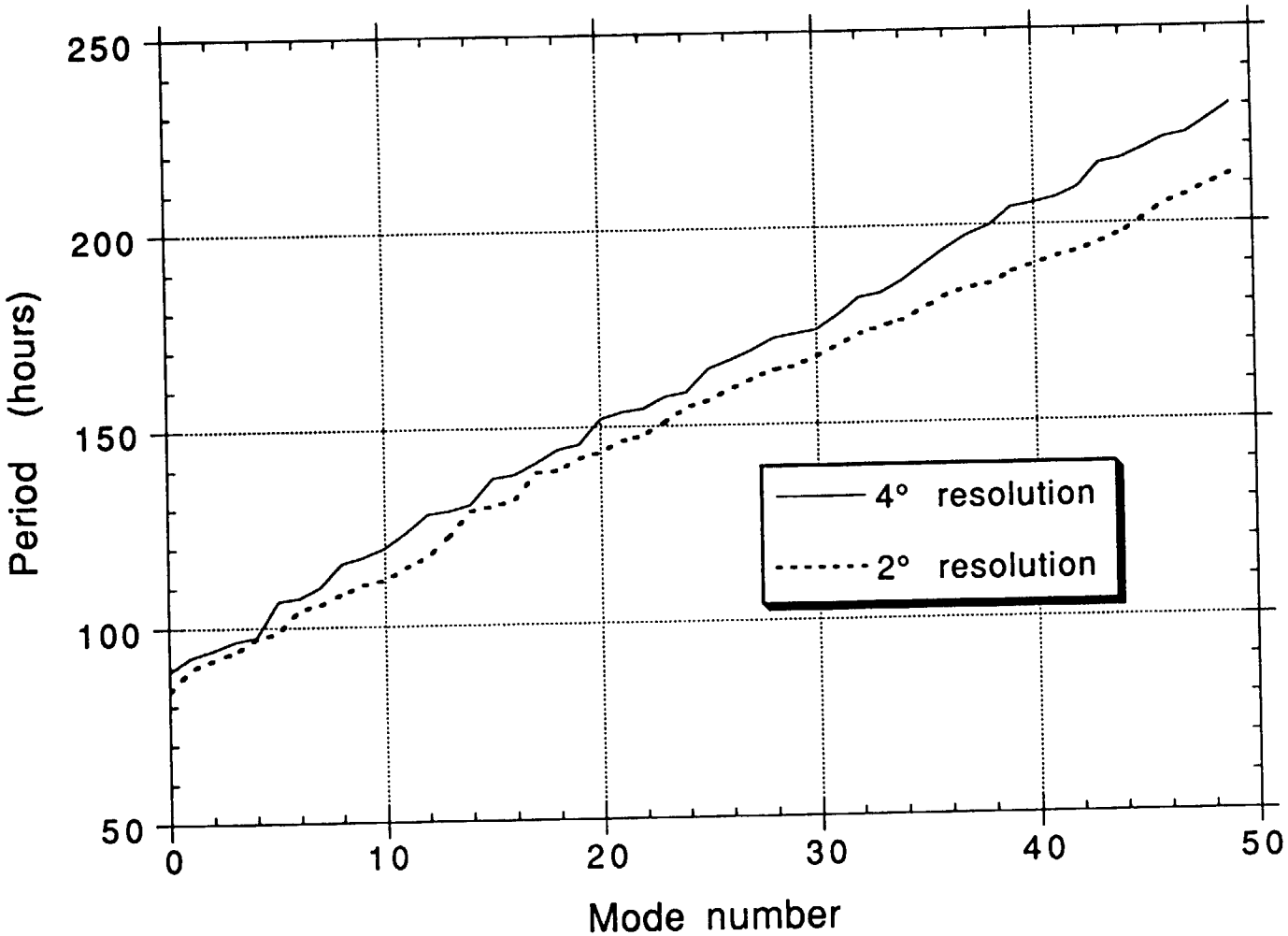

Figure 11. Periods of the rotational modes for the 2–degree and 4–degree solutions.

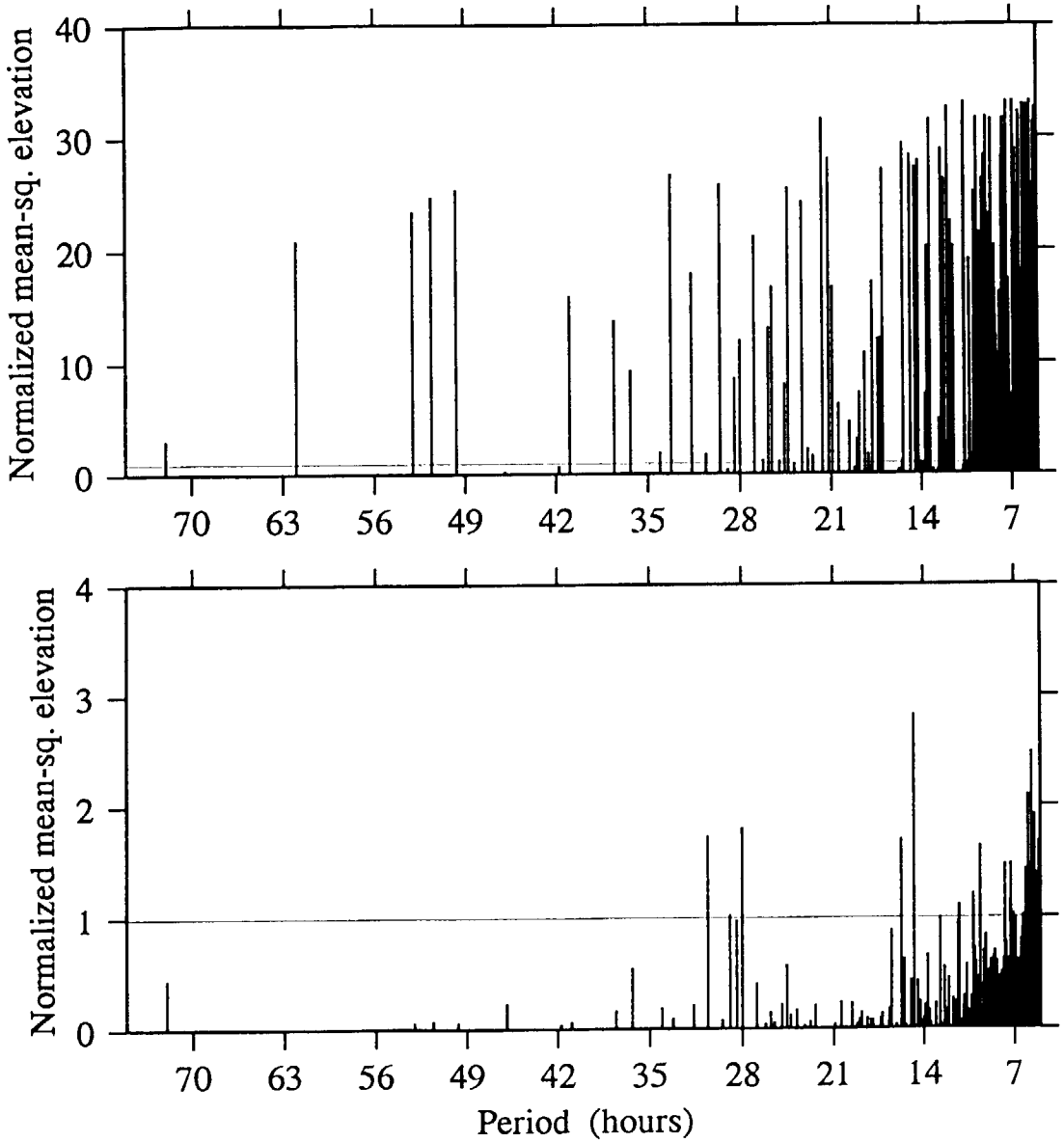

Figure 12. Normalized regional mean–square elevation for the slowest 300 gravity modes, 2–degree solution. *Bottom panel:* South Pole cap extending to 10 degrees north of the Antarctic Circle. *Top panel:* North Pole cap defined by the Arctic Circle.

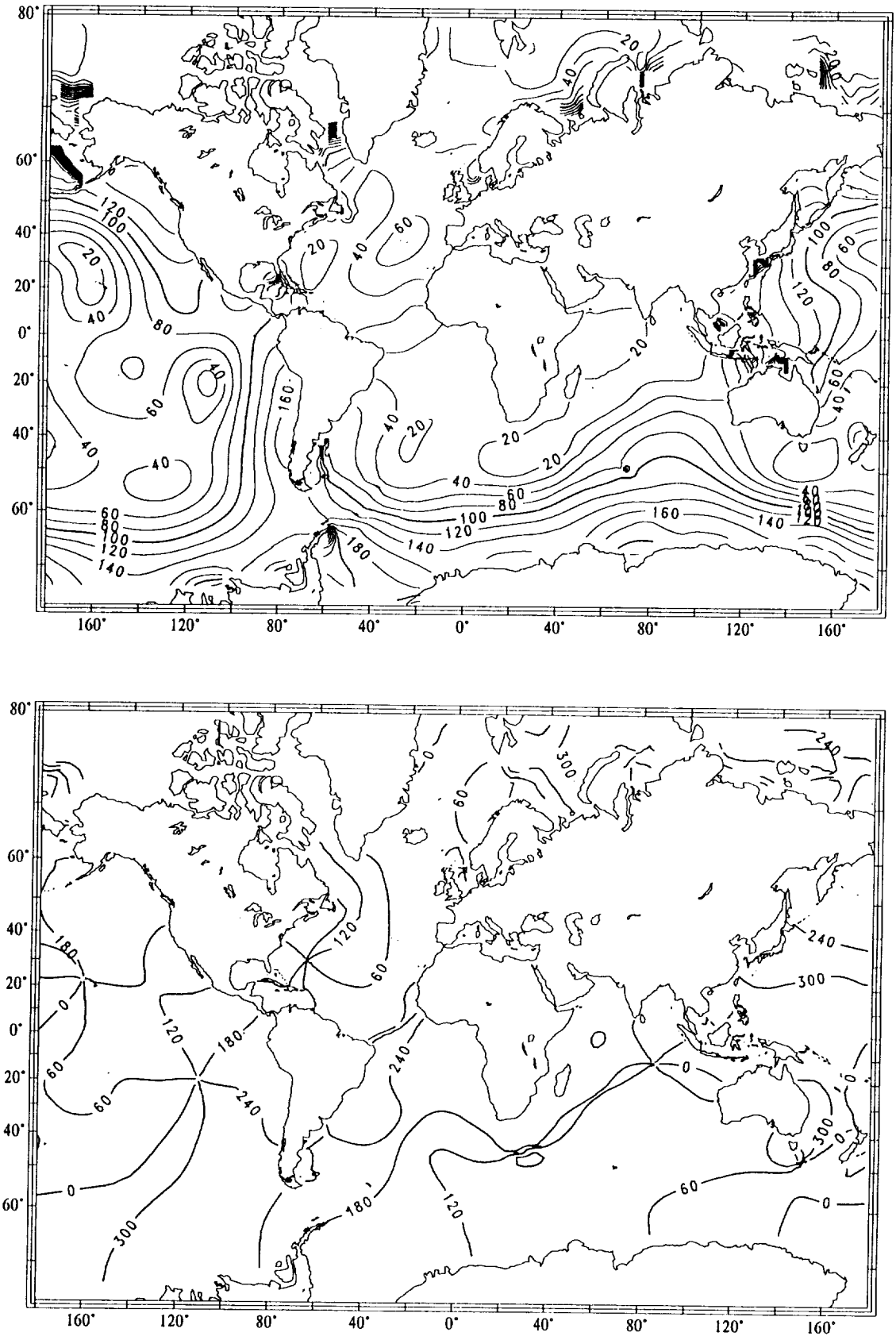

Figure 13. Amplitude and phase for gravity mode number 16, 2-degree solution. Period of 30.57 hours. Amplitude (top panel) normalized to RMS elevation equal to 100. Phase (bottom panel) in degrees. Zero phase assigned to grid point closest to Gibraltar.

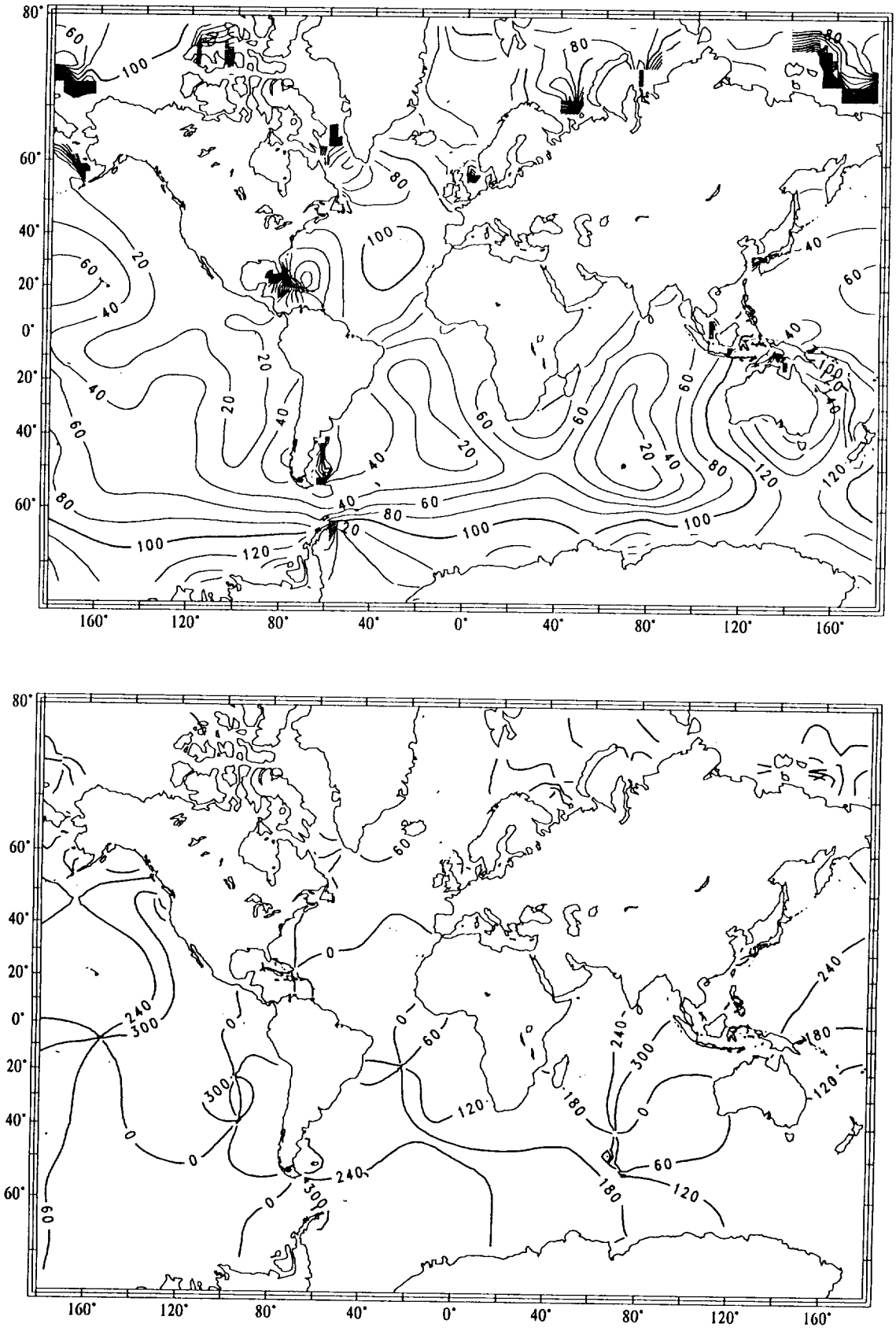

Figure 15. Amplitude and phase for gravity mode number 19, 2–degree solution. Period of 28.40 hours.

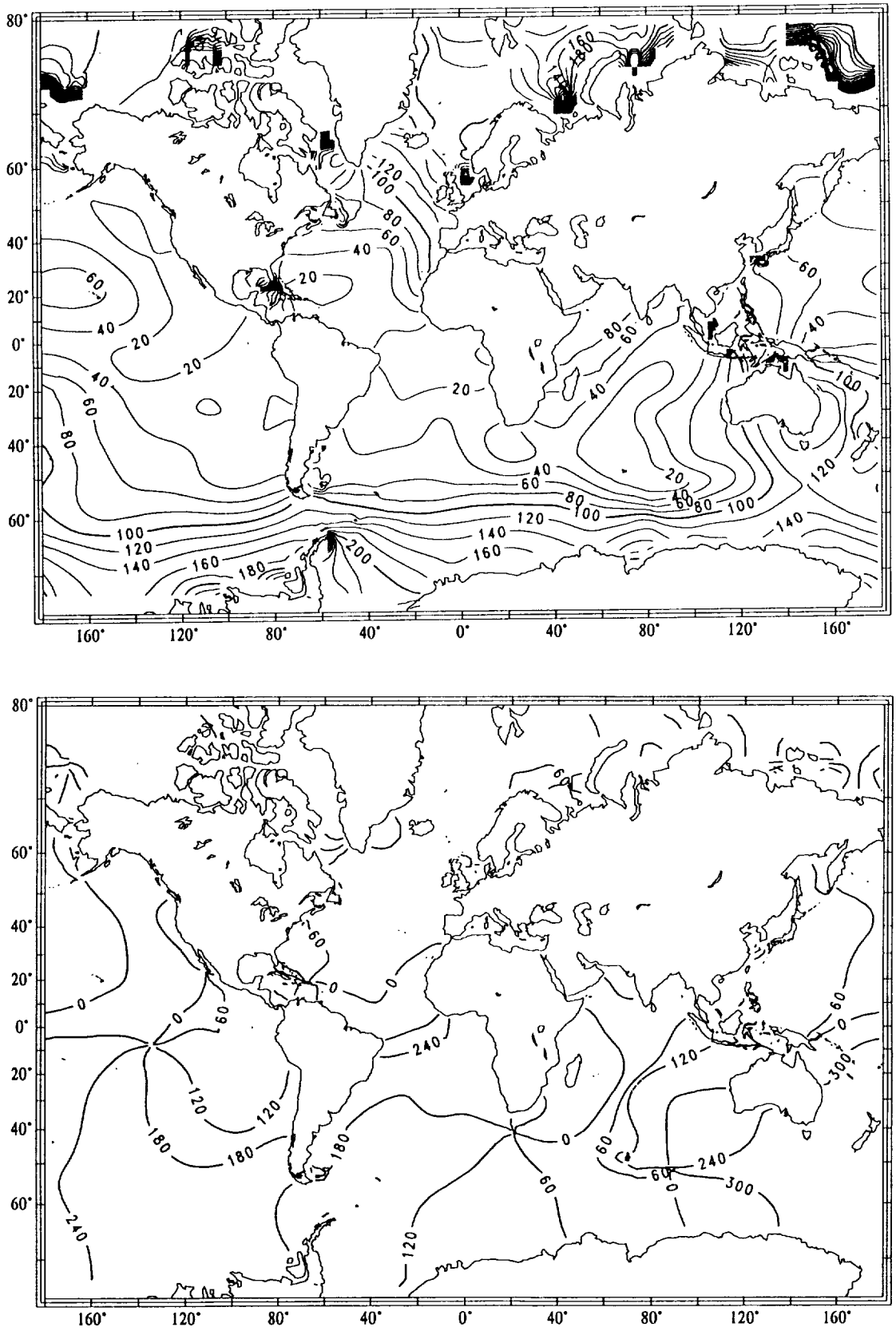

Figure 16. Amplitude and phase for gravity mode number 20, 2-degree solution. Period of 27.99 hours.

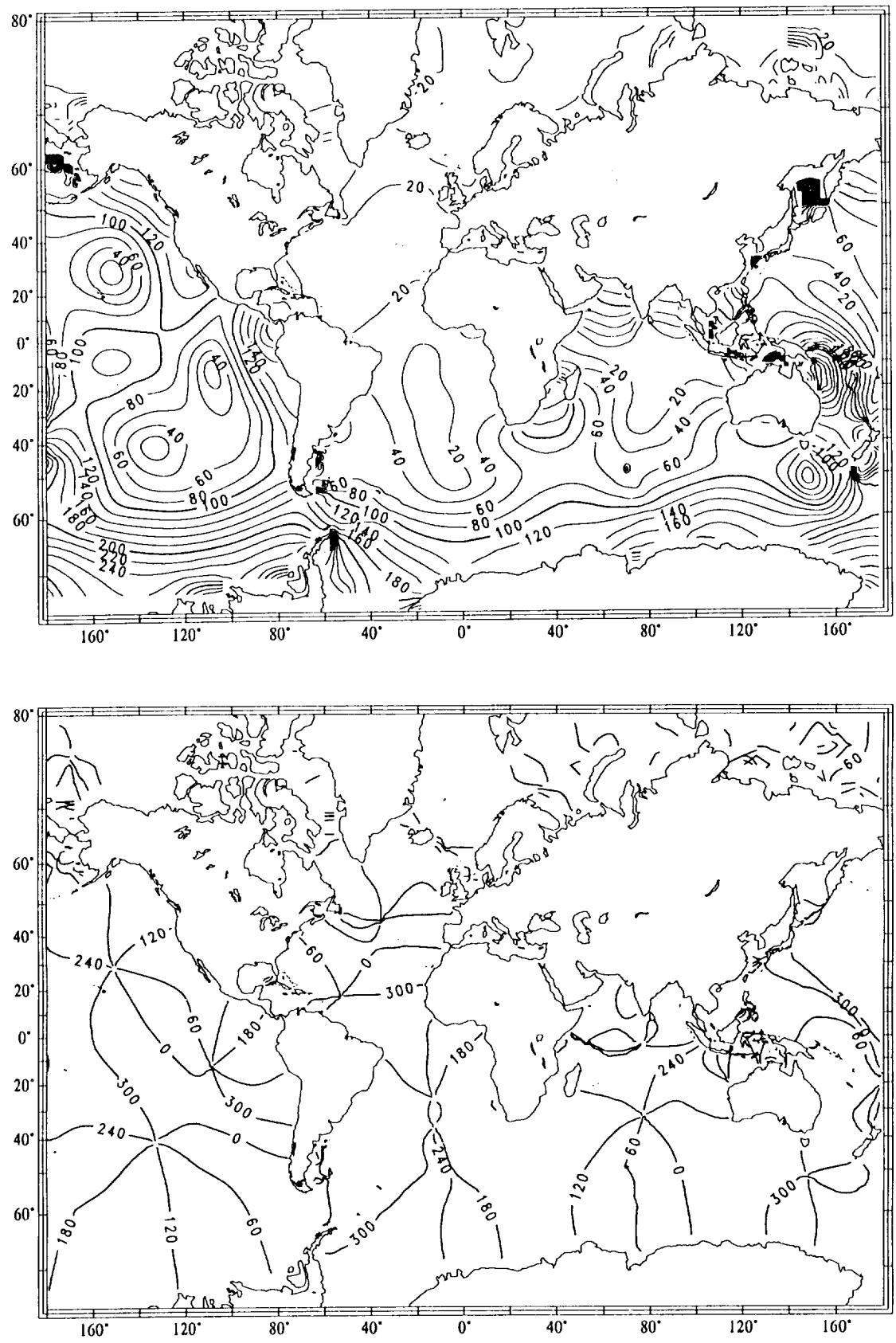

Figure 17. Amplitude and phase for gravity mode number 56, 2–degree solution. Period of 14.71 hours.

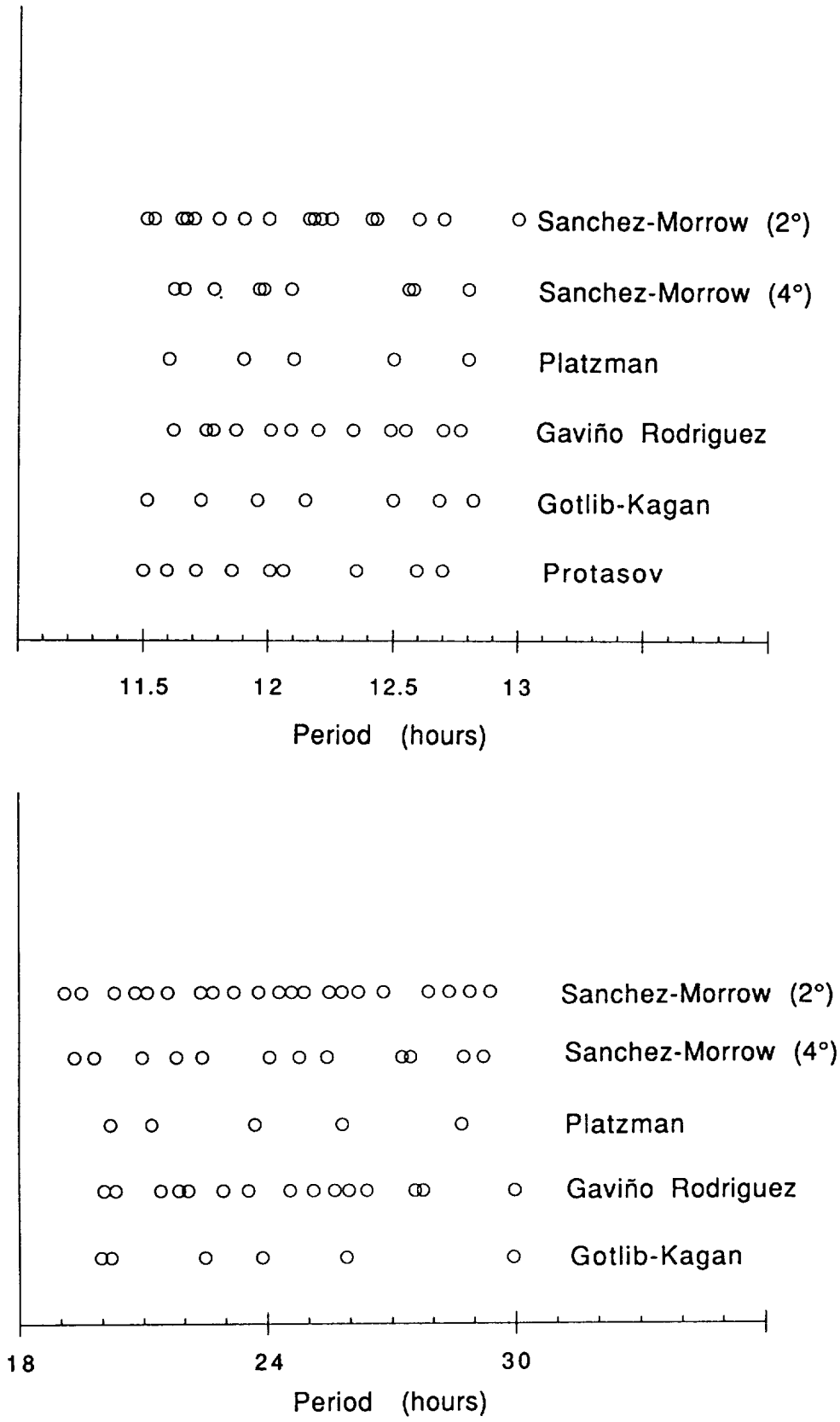

Figure 18. Periods of the gravity modes as obtained by various investigations. *Top panel:* 11.5–13.0 hours range. *Bottom panel:* 19.0–30.0 hours range.

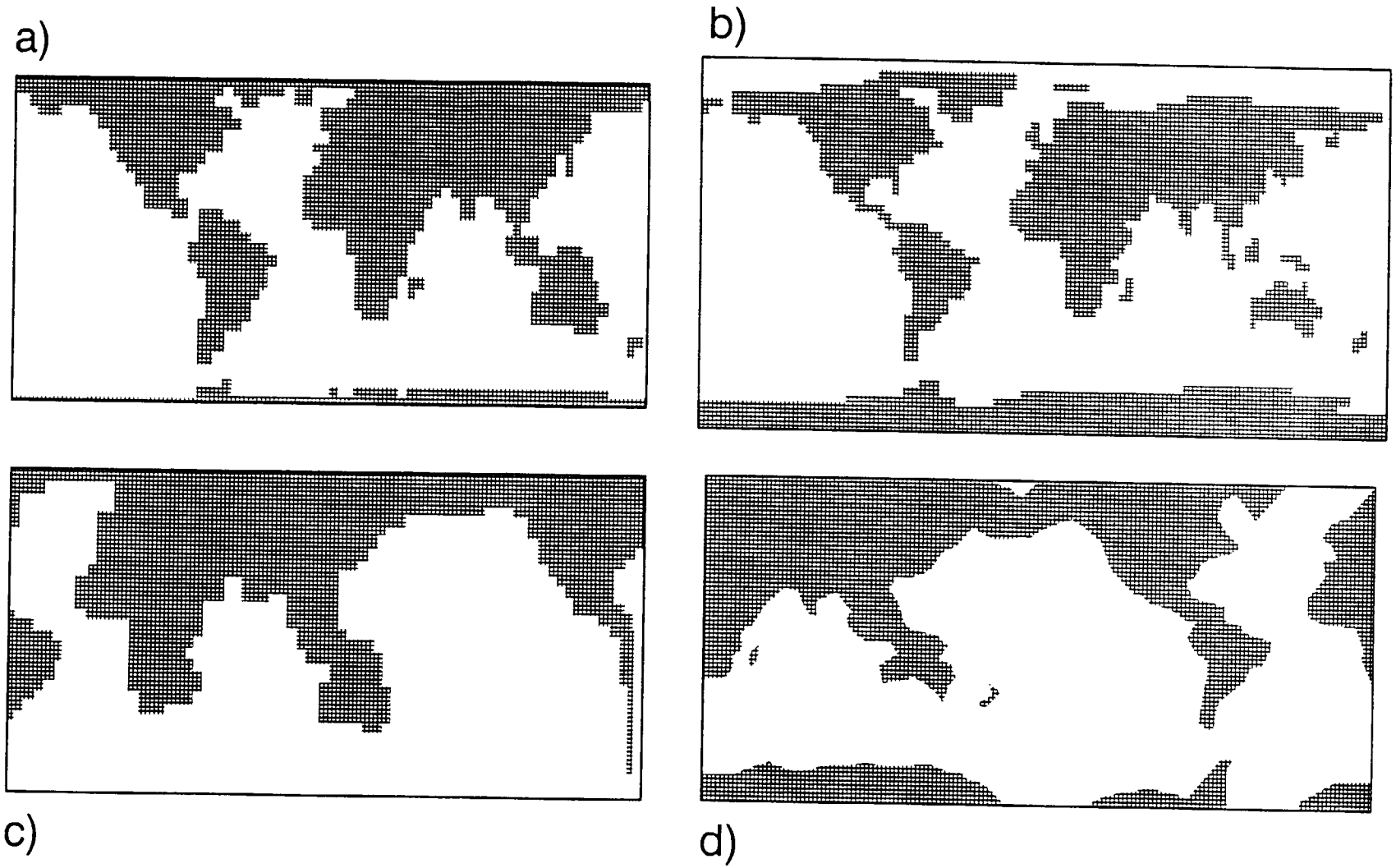

Figure 19. Ocean boundaries of various models. a) Gotlib–Kagan (1981); b) Gaviño Rodriquez (1984); c) Protasov (1979); d) Platzman (1981).

REPORT DOCUMENTATION PAGE

Form Approved
OMB No. 0704-0188

1. AGENCY USE ONLY *(Leave blank)*	2. REPORT DATE	3. REPORT TYPE AND DATES COVERED
	May 1993	Technical Memorandum

4. TITLE AND SUBTITLE

Normal Modes of the World's Oceans, A Numerical Investigation Using Proudman Functions

5. FUNDING NUMBERS

926

6. AUTHOR(S)

Braulio V. Sanchez and Dennis Morrow

7. PERFORMING ORGANIZATION NAME(S) AND ADDRESS(ES)

Goddard Space Flight Center
Greenbelt, Maryland 20771

8. PERFORMING ORGANIZATION REPORT NUMBER

93B00078

9. SPONSORING/MONITORING AGENCY NAME(S) AND ADDRESS(ES)

National Aeronautics and Space Administration
Washington, D.C. 20546–0001

10. SPONSORING/MONITORING AGENCY REPORT NUMBER

TM–104587

11. SUPPLEMENTARY NOTES

Dennis Morrow: Cray Research, Inc., Beltsville, Maryland, 20705.

12a. DISTRIBUTION/AVAILABILITY STATEMENT

Unclassified–Unlimited
Subject Category 48
Report is available from the National Technical Information Service, U.S. Dept. of Commerce, 5285 Port Royal Road, Springfield, VA 22151; (703) 557–4650.

12b. DISTRIBUTION CODE

13. ABSTRACT *(Maximum 200 words)*

This work deals with the numerical modeling of the normal modes of the global oceans. The results of such modeling could be expected to serve as a guide in the analysis of observations and measurements intended to detect these modes. The numerical computation of normal modes of the global oceans is a field in which several investigations have obtained results during the past 15 years. The results seem to be model–dependent to an unsatisfactory extent. This work addresses some modeling areas, such as higher resolution of the bathymetry, inclusion of self–attraction and loading, the role of the Arctic Ocean, and systematic testing by means of diagnostic models. The results show that the present state of the art is such that a final solution to the normal mode problem still lies in the future. The numerical experiments show where some of the difficulties are and give some insight as to how to proceed in the future.

14. SUBJECT TERMS

Numerical Modeling, Supercomputers, Geodesy, Global Ocean, Applied Mathematical Physics, Gravitational Forces (tides), Bathymetry

15. NUMBER OF PAGES

50

16. PRICE CODE

17. SECURITY CLASSIFICATION OF REPORT	18. SECURITY CLASSIFICATION OF THIS PAGE	19. SECURITY CLASSIFICATION OF ABSTRACT	20. LIMITATION OF ABSTRACT
Unclassified	Unclassified	Unclassified	Unlimited